Eigenmodes of spin vertical-cavity surface-emitting lasers with local linear birefringence and gain dichroism

T. Fördös,[1,3,4] H. Jaffrès,[2,*] K. Postava,[3,4] M. S. Seghilani,[5] A. Garnache,[5] J. Pištora,[3] and H. J. Drouhin[1]

[1]*Laboratoire des Solides Irradiés, École Polytechnique, Université Paris-Saclay, F-91767 Palaiseau Cedex, France*
[2]*Unité Mixte de Physique Centre National de la Recherche Scientifique, Thales and Université Paris-Sud,*
1 Avenue A. Fresnel, F-91767 Palaiseau Cedex, France
[3]*Nanotechnology Centre, Technical University of Ostrava, 17 listopadu 15, 708 33 Ostrava, Poruba, Czech Republic*
[4]*IT4 Innovation, Technical University of Ostrava, 17 listopadu 15, 708 33 Ostrava, Poruba, Czech Republic*
[5]*IES, Centre National de la Recherche Scientifique, UMR5214, Université Montpellier, 34090 Montpellier, France*

We present a general method for the modeling of semiconductor lasers such as a vertical-cavity surface-emitting laser and a vertical-external-cavity surface-emitting laser containing multiple quantum wells and involving anisotropies that may reveal (i) a local linear birefringence due to the strain field at the surface or (ii) a birefringence in quantum wells due to phase amplitude coupling originating from the reduction of the biaxial D_{2d} symmetry group to the C_{2v} symmetry group at the III-V ternary semiconductor interfaces. From a numerical point of view, a scattering S-matrix recursive method is implemented using a gain or amplification tensor derived analytically from the Maxwell-Bloch equations. It enables one to model the properties of the emission (threshold, polarization, and mode splitting) from the laser with multiple quantum well active zones by searching for the resonant eigenmodes of the cavity. The method is demonstrated on real laser structures and is presently used for the extraction of optical permittivity tensors of surface strain and quantum wells in agreement with experiments. The method can be generalized to find the laser eigenmodes in the most general case of circular polarized pumps (unbalance between the spin-up and spin-down channels) and/or dichroism allowing an elliptically polarized light emission as recently demonstrated experimentally when the linear birefringence is almost compensated [Joly *et al.*, Opt. Lett. **42**, 651 (2017)].

I. INTRODUCTION

In the past decade, continuous research efforts have been devoted to the physics and to the development of spin lasers as a source of coherent light with enhanced performances (for a recent review, refer, e.g., to Ref. [1]). Spin lasers introduce strong nonlinearities at the laser threshold enabling a kind of amplification of the spin information with a spin-controlled carrier injection. Spin lasers would provide a number of advantages over conventional vertical-cavity surface-emitting lasers (VCSELs) for future optical communication systems such as spin driven reconfigurable optical interconnects [2], fast modulation dynamics [3,4], and polarization control [5,6] as well as higher performances such as laser threshold reduction [7,8], improved laser intensity, and polarization stability. Laser threshold reduction was observed in these devices [7,9,10] and explained theoretically [8,11,12]. Additionally, they have been shown to exhibit a polarization emission that is much more directional than conventional side-emitting laser diodes.

Currently, there exist two kinds of surface-emitting semiconductor lasers: highly integrated monolithic microcavity-type VCSELs that allow low current threshold devices and vertical-external-cavity surface-emitting lasers (VECSELs). Moreover, optical [5,13–15] and electrical [6,16] spin injection were already achieved in monolithic VCSEL structures. A clear control of the laser polarization via optical spin injection was also demonstrated [5,13,17]. In particular, experimental investigations showed that the output circular polarization degree can exceed the input one *via* nonlinear gain effects [13]. Even more recently, a clear controllable elliptically polarized laser emission was demonstrated in VECSELs via circular optical pumps once the intrinsic linear birefringence of the device is compensated [18]. Quantum well VECSELs are very promising solutions for spin lasers along with a class-A dynamics low noise regime [19,20]. For spin-laser functionality, optically pumped III-V semiconductor VECSEL technology is a candidate of choice due to its inherent easier control of in-plane isotropy of material optical properties. Typically, resonant optical cavities of VECSELs are made of a semiconductor chip, an external output coupler, a Bragg reflector, and a multiple quantum well (MQW) [21] or quantum dot gain medium.

Additional anisotropies in the cavity, e.g., linear birefringence or linear gain anisotropy, generally result, however, in preferential linearly polarized laser emission (see, e.g., the results presented in Ref. [18]) and also lead to an additional coupling between modes. These impact on the polarization dynamics of the electrically pumped VCSEL [22–24] by pinning the polarization mode to a certain linearly polarized state [10,25–30]. The dynamics of the circular polarization degree experiences very fast oscillation in the gigahertz range, much faster than the relaxation oscillation [31]. This results in mode beating [4] involving two main frequencies the splitting of which is tuned by the birefringence.

From the pure quantum-mechanical point of view, the optical gain involves an electron-hole recombination process governed by the optical selection rules for dipolar transitions. This is associated with the conservation of the angular momentum in active media or QWs. From the material engineering

---

*Corresponding author: henri.jaffres@cnrs-thales.fr

043828-1

point of view, binary (GaAs, InP, GaN) and ternary (InGaAs, GaAsP) III-V compounds enable radiative recombination of the out-of-equilibrium spin-polarized carriers pumped or electrically injected. The Maxwell-Bloch equations, refined in terms of the so-called spin-flip model (SFM) in the mid-1990s [25,32], describe their dynamics. The evaluation of the gain properties in multilevel systems possibly involving multiple lasing optical transitions has recently been proposed using the steady *ab initio* laser theory (SALT) [31,33,34]. However, what is missing in the latter approach is an evaluation of the optical gain properties involving the spin degree of freedom together with and its possible anisotropy due to the symmetry breaking between the respective in-plane [110] and [1$\bar{1}$0] crystallographic axes as demonstrated recently [35]. In practical situations, a possible way of considering a gain anisotropy is to include differential optical losses [25,32], without, however, being able to correctly describe additional mode coupling. An alternative method, proposed here, is to determine the exact properties of the dipolar interband transitions from the relevant *ab initio* orbital bonding at interfaces. Gain anisotropy may also lead to a generation of mode splitting as observed recently [36–38]. The need for a full microscopic understandings and fundamentals of (spin) VCSELs sets the necessity to consider the particular role of linear and circular anisotropies (circular pumps) on the properties of the polarization emission [22,39] competing with any local host birefringences (surface strain and interfaces).

In this paper we propose to develop a detailed theoretical and computational description of the emission properties of optically active multiple quantum well semiconductor spin lasers (spin VCSELs) in finding the properties of eigenmodes vs selected layer birefringence and optical gain anisotropy in single mode or dual frequency operations. This is performed by considering a quantum-mechanical model for the calculation of the optical gain involving native linear anisotropy and possible elliptically polarized carrier injection together with layer-by-layer electromagnetic wave propagation within the optically anisotropic multilayered semiconductor cavities. We will only consider dual coupling between two transverse modes in dual frequency operation as recently investigated in a series of experiments [40–44]. We do not consider multifrequency laser operations involving several sets of longitudinal modes (Refs. [45,46]) together with their possible coupling because they are characterized by the same polarization properties. By this way, the coupling between longitudinal modes in multifrequency operation should not lead to polarization beating in the time domain like we will consider here.

The paper is organized as follows. In Sec. II, we demonstrate the generalization of the Maxwell-Bloch equations including linear gain dichroism and analytically derive the laser eigenmodes and the gain matrix which affects the electric-field amplitude crossing the active zone. Then, in Sec. III, we introduce matrix formalism with recursive calculation which enables us to model the emission and the electromagnetic wave propagation between multiple QWs and find the eigenmodes and resonance conditions. A clear demonstration of the method is presented in Sec. IV on two real 1/2-VCSEL structures (a laser with a half-integrated resonator and half-external one with a ternary alloyed QW) with linear birefringence and linear

gain dichroism. The anisotropic permittivity tensors of surface and QWs are extracted from the experimental results by using fitting analysis. The formalism can be applied in the future to the emission of circularly polarized emission under electrical or optical spin pumps.

II. PHYSICAL AND MATERIAL PROPERTIES OF THE VECSEL AND 1/2 VECSEL

A. Generalized Maxwell-Bloch equations with linear anisotropies

The carrier-photon dynamics of spin lasers may then be modeled, from the basis of the Maxwell-Bloch equations [31,33,34,45–51], using a spin-dependent rate equation analysis. The rate equations can provide a direct relation between material properties and device parameters [3,12,52]. Generally, a common dynamic SFM originally developed by San Miguel and coworkers two decades ago is used to describe the left- or right-handed polarization switching and bistability [25,32,50]. The polarization properties of the light generated by VCSELs depend on the quantum numbers of the angular momentum in the electronic states between which the optical transitions take place generally under local strain fields. One possibility of considering anisotropy is a generalization of the equations with the considerable simplification of neglecting the longitudinal variations within the system, by taking the z average (where z is the direction of propagation of light) of the optical constant in order to develop the equivalent of the mean-field model in the 2×2 Jones vector analysis [39]. Such an approach, although first satisfactory, prevents a full multiscale description treating the exact effect of the local strain field on the optical birefringence and of the gain. The full scattering matrix method [53,54] developed in this paper fulfills all these requirements.

The Maxwell-Bloch dynamical equations link the electric field **E** and the medium polarization **P** in a vectorial form vs the spin-dependent carrier density, which may be different, using electrical or optical elliptically polarized pumps. The Maxwell-Bloch equations derive from the evolution of the density matrix [33,34,47–50] under the action of the electrical dipolar Hamiltonian $\mathbf{H}_d = -\mathbf{E} \cdot \mathbf{d}$, where $\mathbf{d} = \frac{1}{V}\sum_{(m)} e \cdot \mathbf{r}_{(m)}$ is the host vector dipole moment of the electrons with the charge e and the position vectors $\mathbf{r}_{(m)}$ in the volume V and space coordinate m ($m = x = [100], y = [010], z = [001]$). In the case of the i-polarized electric field $\mathbf{E}_i$ it takes the form $\mathbf{H}_d = -\sum_i \mathbf{E}_i \hat{d}_i$ with the off-diagonal matrix elements between two levels $|1\rangle$ and $|2\rangle$, with $\mu \equiv d_{21,i} = \langle 1|\hat{d}_i|2\rangle$ as the dipolar coupling coefficient. In the slowly varying amplitude approximation limit, rate equations for the dynamics of the electric field **E** and carrier density can be determined once one admits that the medium polarization **P** adiabatically follows the electric-field dynamics according to $\mathbf{P} = \hat{\chi}\mathbf{E}$ ($\hat{\chi}$ is the susceptibility tensor). One admits here that the transverse relaxation time of the optical polarizability is very short corresponding to the main class-A and class-B lasers [55]. In the semiconductor host constituting the optical cavity **E** and **P** are linked by the dielectric constant (or optical refractive index) that we will consider locally via a layer-by-layer approach.
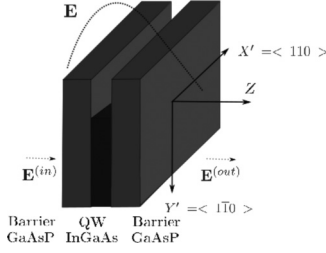
FIG. 1. Scheme of the quantum well and barrier system with crystal axes.

However, crystallographic and electro-optical anisotropies can cause the directions of the vectors **E** and **P** to slightly differ in the active regions where carrier recombination takes place. Even if the resulting optical gain only represents a small fraction of the electromagnetic wave intensity in the cavity, the noncollinearity property between **E** and **P** in QWs is of first importance to understand polarizations and mode coupling. Although beyond the scope of the present paper, the noncollinearity between **E** and **P** also impacts on the competition between circular pumps and native linear gain anisotropy as observed in recent experiments [18,56].

We propose to tackle the problem of noncollinearity between **E** and **P** by deriving a certain optical amplification matrix describing the electric field entering the active zone and its emission from the laser. We refer now to the sketch and notations given in Fig. 1. Let us define the electromagnetic field of the two-mode laser $\mathbf{E}_{(1,2)}$ as a sum of two orthogonal coupled lasing eigenmodes $A_{(1,2)}\boldsymbol{\eta}_{(1,2)}$ in the following way:

$$
\begin{aligned}
\mathbf{E} &= \sum_{i=1,2}\mathbf{E}_{(i)}\exp[i(\omega_{(i)}t - \mathbf{k}_{(i)}\mathbf{r})] + \text{c.c.} \\
&= \sum_{i=1,2}A_{(i)}\boldsymbol{\eta}_{(i)}\exp[i(\omega_{(i)}t - \mathbf{k}_{(i)}\mathbf{r})] + \text{c.c.}, \quad (1) \\
\mathbf{P} &= \sum_{i=1,2}\mathbf{P}_{(i)}\exp[i(\omega_{(i)}t - \mathbf{k}_{(i)}\mathbf{r})] + \text{c.c.}, \quad (2)
\end{aligned}
$$

where the $\boldsymbol{\eta}_{(1,2)}$ are the two polarized eigenmodes we are searching for, either (1) or (2); $A_{(i)}(\mathbf{r},t)$ and $\mathbf{P}_{(i)}$ are, respectively, the slowly time-varying envelope amplitude and the polarization $\mathbf{P}_{(i)} = \hat{\chi}\mathbf{E}_{(i)}$ of the mode i ($i = 1,2$); and $\mathbf{k}_{(i)}$ is the wave vector. In the following, we consider wave propagation parallel to the z direction. The derivation is made by projecting the ongoing electric-field vector of the propagating wave crossing the active region over the two optically active circular reference basis [(+) for spin ↑ and (−) for spin ↓ defined along the direction normal to the layers].

For that purpose, the dipolar amplitude responsible for the optical gain and corresponding to each of the two spin populations has to be derived. We define $\mathbf{A}_{\pm}^d$ as those amplitudes in the Jones vector form largely emphasized in the remaining part of the paper. For a two-level model, we denote $N_{\pm}$ the respective spin-up (+) and spin-down (−) carrier densities in QWs above transparency (tr) where $N_{\pm} = N_{\uparrow\downarrow} - N_{\text{tr}}$ follows the respective pumping rates $N_{0\pm}$. Recent theoretical investigations based on the SALT theory allow an extension from a two-level model to more complex media involving multilevel transitions [33,34]. The dynamical

behavior of each of the physical constituents **E** and **P** follows [47,49]

$$
\begin{aligned}
\frac{\partial \mathbf{P}_{(1,2)}}{\partial t} &= -(\Gamma + i\delta')\mathbf{P}_{(1,2)} - i\frac{\mu^2}{\hbar}[(\mathbf{E}_{(1,2)}\mathbf{A}_+^{d*})\mathbf{A}_+^d N_+ \\
&\quad + (\mathbf{E}_{(1,2)}\mathbf{A}_-^{d*})\mathbf{A}_-^d N_-], \quad (3)
\end{aligned}
$$

$$
\begin{aligned}
\frac{\partial N_{\pm}}{\partial t} &= -\gamma(N_{\pm} - N_{0\pm}) \mp \gamma_s(N_+ - N_-) \\
&\quad - \frac{i}{\hbar}\sum_{i=1,2}\{(\mathbf{E}_{(i)}^*\mathbf{A}_{\pm}^d)(\mathbf{P}_{(i)}\mathbf{A}_{\pm}^{d*}) - \text{c.c.}\}, \quad (4)
\end{aligned}
$$

$$
\begin{aligned}
&\frac{\partial^2}{\partial t^2}\mathbf{P}_{(1,2)}\exp[i(\omega t - k_{(1,2)}z)] \\
&= \left[c^2\,\nabla^2 - \epsilon\frac{\partial^2}{\partial t^2} - \kappa\frac{\partial}{\partial t}\right]\mathbf{E}_{(1,2)}\exp[i(\omega t - k_{(1,2)}z)], \quad (5)
\end{aligned}
$$

where Γ is the off-diagonal damping factor for the off-diagonal density-matrix elements (media polarization), γ is the damping rate of the carrier densities, γ_s is the corresponding spin-flip rate, and δ' is the spectral detuning.

Those three equations represent a generalization of the Maxwell-Bloch equations and of the spin-flip model we were searching for to the case of anisotropic active regions. The difference with previous approaches is now that we have projected the **E** and **P** fields within a nonorthogonal basis imposed by the anisotropy. Indeed, from the first equation, one can be convinced that the *vectorial* optical gain is not necessarily collinear to the incoming **E** field for $\langle\boldsymbol{\eta}_{(2)}|\mathbf{A}_+^d\rangle \neq 0$ and $\langle\boldsymbol{\eta}_{(1)}|\mathbf{A}_-^d\rangle \neq 0$. This feature is reinforced if birefringences within the semiconductor host, e.g., are considered. Our modeling method satisfies the Eqs. (3)–(5) in each of the layers, active regions, barriers, and semiconductor host by using selected optical constants. In particular, the last equation describes the propagation of the electromagnetic field throughout the structure including a certain optical loss. This can be modeled by a certain imaginary part into the dielectric constant tensor (or the optical refractive index) describing a possible temporal damping parameter $\kappa \sim 1/\tau_{\text{layer}}$ where τ_{layer} denotes the photon lifetime. In the following, we will derive the optical gain properties by considering QWs free of losses.

B. Derivation of the optical gain including linear anisotropy

1. Derivation of the optical gain tensor

We are now searching for a general numerical scheme for the determination of the resonant eigenmodes in cavities. The assumption of the slowly variable amplitude approximation and of a fast polarization damping leads, in a steady-state operation regime, to

$$
\frac{\partial \mathbf{E}_{(i)}}{\partial t} = -\frac{1}{2}\kappa\mathbf{E}_{(i)} + i\frac{\omega}{2\epsilon}\mathbf{P}_{(i)} \quad (6)
$$

and

$$
\langle\mathbf{P}_{(i)}\rangle = -i\frac{\mu^2}{\hbar}\frac{[(\mathbf{E}_{(i)}\mathbf{A}_+^{d*})\mathbf{A}_+^d N_+ + (\mathbf{E}_{(i)}\mathbf{A}_-^{d*})\mathbf{A}_-^d N_-]}{\Gamma + i\delta'}, \quad (7)
$$

which yields

$$\frac{\partial \mathbf{E}_{(i)}}{\partial t} = -\frac{1}{2}\kappa \mathbf{E}_{(i)} + \frac{\omega \mu^2}{2\epsilon(\Gamma + i\delta')}[(\mathbf{E}_{(i)}\mathbf{A}_+^{d*})\mathbf{A}_+^d N_+$$
$$+ (\mathbf{E}_{(i)}\mathbf{A}_-^{d*})\mathbf{A}_-^d N_-]. \quad (8)$$

This is the general dynamical equation controlling the change of the **E**-field envelope amplitude in a nonzero polarization medium. It gives then the expression for the field amplification in an active layer (QWs) once the spin-polarized carrier densities $N_\pm$ are given. A slow dynamics of $N_\pm$ may come into play when one considers two or several coupled modes [45,46] or oscillation emission, which we will not consider henceforth. Although we will discuss the impact of anisotropies on a possible two transverse mode coupling, we only address here the issue of a single mode laser and we are searching for such modes.

If one neglects any optical losses in QWs ($\kappa_{\text{QW}} \to 0$), one can implement a fast integration in time [Eq. (6)] leading thus to the required jump in $\delta \mathbf{E}_{(i)}$ according to $\delta \mathbf{E}_{(i)} = \frac{nW\omega\mu^2}{2c\epsilon(\Gamma+i\delta)\hbar}[(\mathbf{E}_{(i)} \cdot \mathbf{A}_+^{d*})\mathbf{A}_+^d N_+ + (\mathbf{E}_{(i)} \cdot \mathbf{A}_-^{d*})\mathbf{A}_-^d N_-]$ with the result

$$\delta \mathbf{E}_{(i),m} = g_0 \mathcal{T}_{mn} \mathbf{E}_{(i),n}, \quad (9)$$

where

$$\mathcal{T}_{mn} = \left[\mathbf{A}_{+,m}^{d*}\mathbf{A}_{+,n}^d \frac{N_+}{N_+ + N_-} + \mathbf{A}_{-,m}^{d*}\mathbf{A}_{-,n}^d \frac{N_-}{N_+ + N_-}\right]. \quad (10)$$

W represents the QW thickness and $\mathcal{T}$ is the *optical gain tensor* for the electromagnetic field $\mathbf{E}_{(i)}$ with a corresponding gain amplitude equaling

$$g_0 = \frac{nW\omega\mu^2 N}{2c\epsilon(\Gamma + i\delta)\hbar}, \quad (11)$$

where $N = N_+ + N_-$ is the total pumped carrier density above transparency and the NW product represents the carrier sheet density in QWs. We recall that the subscripts (m,n) are the space coordinates. As discussed in the following, this particular form of the gain we derived should include the phase-amplitude coupling known as the Henry factor $\alpha = \frac{\text{Real}(\partial\chi/\partial N)}{\text{Im}(\partial\chi/\partial N)}$ [$\equiv \frac{\delta}{\Gamma}$ and where $\chi(\omega)$ is the matter susceptibility]. In that sense, g_0 may be written as $g_0 = g_{00}(1 - i\alpha)$. The relevance of the so-called Henry's factor also manifests on the steady-state SALT equations described in Refs. [33,34]. Equation (9) simply reflects an amplification of the m component ($m = x,y$) of the **E** field for an incoming n component ($n = x,y$) when $N_\pm$ are controlled parameters at present (Fig. 1). Off-diagonal components of the $\mathcal{T}$ matrix reflect the noncollinearity between dipole sources and eigenmodes, originating from the linear gain dichroism. The particular expression for the prefactor gain g_0 is the one given at low out-of equilibrium carrier densities from which it should be generalized into

$$g_0 = \frac{n\omega\mu^2}{2c\epsilon(\Gamma + i\delta)\hbar}(N_{\text{th}}W)\ln\left(\frac{N + N_s}{N_{\text{th}} + N_s}\right), \quad (12)$$

giving $g_0(N) \simeq \frac{\partial g_0}{\partial N}N$ with the differential gain $\frac{\partial g_0}{\partial N}$. Here N_{th} is the carrier density at threshold (or slightly smaller) and N_s is

an adjustable parameter controlling the correct gain variation with N [57].

In order to derive the expression of the 2×2 optical gain tensor $\mathcal{T}_{ij}$, one needs to consider the two different **E**-field polarization sources, $\mathbf{A}_\pm^d$ within the active regions (QWs). These are described in a Jones vector form and correspond separately to the two different spin eigenchannels, respectively, $+$ and $-$. Due to the quantization axis of the wave functions, along the z direction normal to the layers, the correct basis is the $\pm$ spin basis along z even in the case of a linearly polarized pump (the particular case with $N_+ = N_-$). $\mathbf{A}_\pm^d$ are complex conjugate from each other $\mathbf{A}_-^d = (\mathbf{A}_+^d)^*$ but not necessarily orthogonal.

2. Effect of the linear gain anisotropy

We consider now the possible case of a linear gain anisotropy in the active layers (QWs), imposed by a certain bonding anisotropy at the interface with the barriers due to the symmetry reduction from D_{2d} to C_{2v}. The overall gain anisotropies may be characterized by (i) a Δ parameter departing from 1 (we will see in the following that $\Delta = 1$ will correspond to a perfect isotropy) and (ii) the effective spin polarization in QWs of carriers pumped, $\mathcal{P}_s = \frac{N_+ - N_-}{N_+ + N_-}$. The evaluation of $\mathbf{A}_\pm^d$ is performed in the $X' = [110], Y' = [1\bar{1}0]$ crystallographic basis for the two reference optical directions. Associated to a possible anisotropy of the optical oscillator strengths along X' and Y', two different dipolar transition matrix elements can be ascribed for an **E** emission along X' or Y' according to $\Pi_{x'} = \langle S|p_{x'}|X'\rangle = -i\hbar\langle S|\nabla_{x'}|X'\rangle$ and $\Pi_{y'} = \langle S|p_{y'}|Y'\rangle = -i\hbar\langle S|\nabla_{y'}|Y'\rangle$ with $\Pi_{y'} = \Delta\Pi_{x'}; \Delta \neq 1$ then refers to a certain linear gain anisotropy. $\hat{p}_m$ is the impulsion operator and Π_m is the corresponding optical transition element. We refer, e.g., to the notation of Faria, Jr. *et al.* [58] for the description of the respective S (conduction band) and X, Y, and Z (**P**-type orbitals of the valence band) quantum states describing the optical interband dipolar terms. We find that

$$\mathbf{A}_+^d = \frac{1}{\sqrt{1 + \Delta^2}}\begin{bmatrix}(1 + \Delta)/2 - i(1 - \Delta)/2 \\ -i(1 + \Delta)/2 + (1 - \Delta)/2\end{bmatrix} \quad (13)$$

and $\mathbf{A}_-^d = (\mathbf{A}_+^d)^*$ for the respective spin $\uparrow$ ($+$) and spin $\downarrow$ ($-$) channels. $\mathbf{A}_\pm^d$ are complex conjugate from each other. Nonetheless, they are generally not orthogonal in the presence of certain linear gain anisotropy. The two measurable optical laser polarization eigenmodes derived from the diagonalization of the optical $\mathcal{T}$ matrix, $\boldsymbol{\eta}_\pm$, are then orthogonals. It may result in a nonorthogonality between $\mathbf{A}_\pm^d$ and $\boldsymbol{\eta}_\pm$ as depicted in Fig. 2. This is the source of a strong mode coupling between the two transverse modes.

The resulting dipolar amplification matrix $\mathcal{T}$ in Eq. (10) is given by

$$\mathcal{T} = g_{00}(1 - i\alpha)\begin{bmatrix}\frac{1+\Delta^2}{2} & \frac{1-\Delta^2}{2} - i\mathcal{P}_s\Delta \\ \frac{1-\Delta^2}{2} + i\mathcal{P}_s\Delta & \frac{1+\Delta^2}{2}\end{bmatrix}, \quad (14)$$

where $g_{00}(1 - i\alpha)$ is the optical gain parameter. The **E** field in the QW obeys $\mathbf{E}^{(\text{out})} - \mathbf{E}^{(\text{in})} = g_{00}(1 - i\alpha)\mathcal{T}\mathbf{E}^{(\text{in})}$ or $\mathbf{E}^{(\text{out})} = \mathbf{T}\mathbf{E}^{(\text{in})}$ where $\mathbf{T} = I_{2\times2} + \mathcal{T}$ admits an Hermitian form. As discussed before, we have also introduced the phase-amplitude
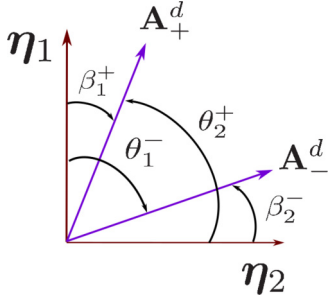
FIG. 2. Scheme of the two orthogonal laser eigenmodes $\eta_{1,2}$ and dipolar source vectors $\mathbf{A}_\pm^d$. The dipolar source vectors are not necessarily orthogonal to each other depending on the dichroism in play. The nonorthogonality between $\mathbf{A}_\pm^d$ is at the origin of a strong mode coupling as discussed in the text.

Henry's coefficient α [59,60] describing the local change in the optical constant from free carriers. Via a diagonalization procedure of $\mathcal{T}$ (or $\mathbf{T}$), one finds the two different polarized eigenmodes we are searching for, $\eta_{(1,2)}$, together with the optical gain $g_{(1,2)}$ as the corresponding eigenvalues. Those are given vs the spin-polarization of carriers $\mathcal{P}_s$ and the oscillator strength anisotropy Δ:

$$\eta_{(1,2)} = \frac{1}{\sqrt{2}} \left[\begin{array}{c} 1 \\ \pm \dfrac{\frac{1-\Delta^2}{2} - i\mathcal{P}_s\Delta}{\sqrt{\left(\frac{1-\Delta^2}{2}\right)^2 + (\mathcal{P}_s\Delta)^2}} \end{array} \right]_{\langle 100 \rangle}, \tag{15}$$

where the [100] subscript means that the present expression for the modes is expressed in the cubic $\langle 100 \rangle$ reference crystallographic axis. $g_{(1,2)}$ are expressed as

$$g_{(1,2)} = g_0(N_+ + N_-)$$
$$\times \left[\frac{1+\Delta^2}{2} \pm \sqrt{\left(\frac{1-\Delta^2}{2}\right)^2 + \mathcal{P}_s^2\Delta^2} \right] \tag{16}$$

or

$$g_{(1,2)} = g_0(N_+ + N_-)\bar{g}_{(1,2)}. \tag{17}$$

In the above formula giving $g_{(1,2)}$ the $(+)$ sign refers to the mode (1) whereas the $(-)$ sign refers to the mode (2). $\bar{g}_{(1,2)} = \frac{1+\Delta^2}{2} \pm \sqrt{\left(\frac{1-\Delta^2}{2}\right)^2 + \mathcal{P}_s^2\Delta^2}$ are the reduced gains. One recovers $g_{(1,2)} = g_\pm = 1 \pm \mathcal{P}_s$ for $\Delta = 1$ (no linear anisotropy) whereas $g_{(1)} = 1$ and $g_{(2)} = \Delta^2$ for $\mathcal{P}_s = 0$ for the linear polarized pump, as expected. In the more general case, eigenmodes and corresponding gain display a more complex form. However, one can be convinced that the two sets of vectors $\eta_{1,2}$ and $\mathbf{A}_\pm^d$ are generally not collinear to each other, leading to a strong mode coupling between the two transverse modes η_1 and η_2 as discussed below.

3. Coupling between transverse modes

Although not in the scope of the present paper, we discuss here the impact of noncollinearity between $\eta_{1,2}$ and $\mathbf{A}_\pm^d$ on the transverse mode coupling, as sketched in Fig. 2, and leading to possible polarization beating. The possible mode coupling between longitudinal modes [45] of the same polarization is

not considered here because of the absence of any polarization beating. One gets the effective optical gain β_1^+ and β_2^- from the squared projection of the *natural* optical eigenmode polarization along the dipole source direction according to

$$\beta_1^+ = |\langle \eta_{(1)} | \mathbf{A}_+^d \rangle|^2 = \frac{1 + \sin(2\phi_1 + \phi_2)}{2}, \tag{18}$$

$$\beta_2^- = |\langle \eta_{(2)} | \mathbf{A}_-^d \rangle|^2 = \frac{1 - \sin(2\phi_1 - \phi_2)}{2} \tag{19}$$

as depicted in Fig. 2. In the same spirit, the coupling between modes or the *cross-coupling* terms θ_1^- and θ_2^+ [40,42,44], involving linear gain anisotropy now, are calculated from the squared projection of the optical eigenmode polarization along the cross-dipole source direction:

$$\theta_1^- = |\langle \eta_{(1)} | \mathbf{A}_-^d \rangle|^2 = \frac{1 + \sin(2\phi_1 - \phi_2)}{2}, \tag{20}$$

$$\theta_2^+ = |\langle \eta_{(2)} | \mathbf{A}_+^d \rangle|^2 = \frac{1 - \sin(2\phi_1 + \phi_2)}{2} \tag{21}$$

where ϕ_1 and ϕ_2 are given by

$$\phi_1 = \arctan\left(\frac{1 - \Delta}{1 + \Delta}\right), \tag{22}$$

$$\phi_2 = \arctan\left(\frac{2\mathcal{P}_s\Delta}{1 - \Delta^2}\right). \tag{23}$$

It results that θ_1^- and θ_2^+ couple the two mode amplitudes and that this coupling is strongly correlated to the linear gain dichroism Δ and the carrier spin polarization $\mathcal{P}_S$. A zero linear gain dichroism $\Delta = 1$ leads to no-coupling $\theta_{1,2}^{-;+} = 0$ whatever the spin polarization $\mathcal{P}_S$. The increase of the linear gain dichroism ($\Delta < 1$) increases the coupling between modes ($\theta_{1,2}^{-;+} > 0$) even in the case of a nonzero spin polarization $\mathcal{P}_s$. The dynamics of carriers pumped are given by the generalization of Eq. (4):

$$\frac{\partial N_+}{\partial t} = -\gamma(N_+ - N_{0+}) - \gamma_s(N_+ - N_-)$$
$$- \gamma\left(\bar{g}_{(1)}(N)\beta_1^+ \frac{I_{(1)}}{I_{\text{sat}}} + \bar{g}_{(2)}(N)\theta_1^- \frac{I_{(2)}}{I_{\text{sat}}}\right), \tag{24}$$

$$\frac{\partial N_-}{\partial t} = -\gamma(N_- - N_{0-}) + \gamma_s(N_+ - N_-)$$
$$- \gamma\left(\bar{g}_{(1)}(N)\theta_2^+ \frac{I_{(1)}}{I_{\text{sat}}} + \bar{g}_{(2)}(N)\beta_2^- \frac{I_{(2)}}{I_{\text{sat}}}\right) \tag{25}$$

with the field intensity at saturation $I_{\text{sat}} = \frac{\epsilon c \hbar^2 (\Gamma^2 + \delta^2)\gamma}{n\mu^2\Gamma}$. We recover the expression for the dynamics of coupling modes vs the coupling coefficient θ [56,61] from the Lamb model, that we have expressed vs the linear gain dichroism parameter Δ appearing in $\bar{g}_{(1,2)}$, $\beta_{(1,2)}$, and $\theta_{(1,2)}$. In that picture, the overall coupling coefficient $\mathcal{C}$ [40,42,44] between the two transverse intensity modes $I_{(1)}$ and $I_{(2)}$ is written

$$\mathcal{C} = \frac{\theta_1^- \theta_2^+}{\beta_1^+ \beta_2^-}$$
$$= \frac{[1 - \cos(2\phi_1)\sin(\phi_2)]^2 - \sin^2(2\phi_1)\cos^2(\phi_2)}{[1 + \cos(2\phi_1)\sin(\phi_2)]^2 - \sin^2(2\phi_1)\cos^2(\phi_2)}. \tag{26}$$

The simultaneous oscillation of two orthogonally polarized states is ruled by the strength of the nonlinear coupling between the two eigenstates in the active medium. Whether the coupling constant $\mathcal{C}$ is higher or lower than 1 leads, respectively, to two distinct regimes, namely, bistability and simultaneity [40]. We now restrict ourselves to laser modes with linearly polarized optical gain along the [110] and [1$\bar{1}$0] directions and no spin-polarized pump ($\mathbf{P}_s = 0$). In this case, the respective gains are $g_{(1)} = 1$ and $g_{(2)} = \Delta^2$ as expected. These experimental conditions are often fulfilled in real situations with no spin-polarized carrier pump, corresponding to two possible linear modes along [110] and [1$\bar{1}$0] directions.

C. Source of linear birefringence in optical cavities

Vector dipolar sources in active regions of VECSELs do not necessarily force the polarization to be emitted in the same direction because of the residual linear birefringences within the semiconductor multilayers. These anisotropic properties of the dielectric function strongly impact the performance and properties of laser operation leading to the complex polarization dynamics and polarization switching [57]. Previous theoretical and experimental investigations allowed separation between two different contributions. The first anisotropy to consider is the unavoidable linear phase anisotropy induced by a possible local strain field in the material host via electro-optical effects [62,63] and originating, e.g., from the lattice mismatch [22] or from the crystal relaxation at the surface [35,64–66]. As a result, the directional degeneracy between the two in-plane [110] and [1$\bar{1}$0] directions will be removed and the frequencies for the corresponding two linear polarizations will be split. The second source of anisotropy is the linear birefringence originating from the interface between ternary quantum wells and barriers (GaAsP/InGaAs/GaAsP). An in-plane optical anisotropy in III-V QWs was found due to the breakdown of the rotoinversion symmetry at interfaces when the host materials do not share any common atoms (symmetry breaking from D_{2d} to C_{2v}) [65] or due to an In chemical segregation [35]. This optical anisotropy has been evaluated by the pseudopotential microscopic model as well as by $\mathbf{k}\cdot\mathbf{p}$ models including relevant electronic boundary conditions [65,67–69]. Such an effect of linear birefringence in the QWs is generally measured by optical reflectance [70], by optical transmission [71], or by optical absorption [72]. In Sec. III, we will introduce the necessary 4×4 matrix formalism enabling us to describe the wave propagation inside the anisotropic multilayer laser cavity as described by Eq. (5) of the Maxwell-Bloch equations.

III. MODEL FOR EMISSION FROM MULTILAYER LASER STRUCTURE WITH A MULTIPLE QW SOURCE: METHODOLOGY

A. Description of the optical gain in multilayers: The Jones vector formalism

In this section, we describe the main properties of the optical gain tensor derived above and the propagation of the electromagnetic field inside the multilayer laser. One defines the amplitude of the source Jones vector in a Cartesian s-p basis according to $\mathbf{A}_{\text{down}}^d = [A_1^d;\ A_3^d]^T$ and $\mathbf{A}_{\text{up}}^d = [A_2^d;\ A_4^d]^T$
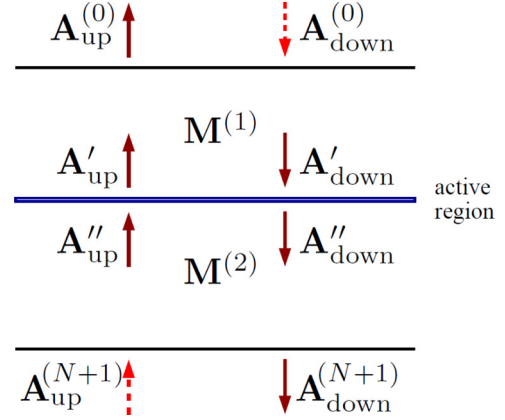

FIG. 3. Schematic description of the structure with a single active layer showing wave propagation inside the cavity.

(with T transpose vectors) as illustrated in Fig. 3. Those describe the $\mathbf{E}$ waves, respectively, propagating downward and upward. We call, respectively, $\mathbf{A}_{\text{up,down}}'$ and $\mathbf{A}_{\text{up,down}}''$ the amplitudes of the $\mathbf{E}$ field traveling towards the respective *up* and *down* directions in the region of space below (") and above (') a given active QW region, as depicted in Fig. 3. Amplification effects by the dipole sources in the active layers can be expressed in the following matrix form:

$$\begin{bmatrix} \mathbf{A}_{\text{up}}' \\ \mathbf{A}_{\text{down}}'' \end{bmatrix} = \begin{bmatrix} \mathbf{T}_{\text{uu}} & \mathbf{0} \\ \mathbf{0} & \mathbf{T}_{\text{dd}} \end{bmatrix} \begin{bmatrix} \mathbf{A}_{\text{up}}'' \\ \mathbf{A}_{\text{down}}' \end{bmatrix} + \gamma_{\text{sp}} \begin{bmatrix} \mathbf{A}_{\text{up}}^d \\ \mathbf{A}_{\text{down}}^d \end{bmatrix}, \quad (27)$$

where the first term describes the stimulated emission involving the amplification tensor $\mathbf{T}_{\text{uu}}$ and $\mathbf{T}_{\text{dd}}$ (*uu* for up-ingoing and up-outgoing and *dd* for down-ingoing and down-outgoing), the precise form of which will be given later. The second term in the right-hand side of the equation describes the spontaneous emission (stochastic process) weighted by the coefficient γ_{sp}.

After reflections on mirrors and back and forth traveling, the wave polarization $\mathbf{A}_{\text{down}}'$ may be different from the source $\mathbf{A}_{\text{down}}^d$ because of residual birefringences (linear or circular) in the host. Note also that, for elliptical modes, polarization and Jones vectors are changed after reflection on Bragg mirrors and output mirror (coupler) leading to the definition of two different optical-gain tensors for up- and down-propagation. The result [54] is that one has to consider the gain tensor, $\mathcal{T}_{mn}^{\alpha\beta}$, in a supermatrix form with double index, one $m,n = x,y,z$ for the coordinates and the other $\alpha,\beta = uu,dd$ for the propagation direction *(up, down)*. In that sense, *(up,up)* means amplification from an *up-incoming* wave into an *up-outgoing* wave, and similarly for *(down,down)* combination.

Considering normalized vector sources, $(\mathbf{A}_{\text{down}}^d)^+ \mathbf{A}_{\text{down}}^d = 1$, $\mathbf{T}_{\text{uu}}$ and $\mathbf{T}_{\text{dd}}$ admit the form

$$\mathbf{T}_{\text{uu}} = \mathbf{I} + g_{00}[1 - i\alpha\mathcal{T}_{\text{uu}}]\mathcal{T}_{\text{uu}} \quad (28)$$

with

$$\mathcal{T}_{\text{uu}} = \begin{bmatrix} A_2^d A_2^{d*} & A_2^d A_4^{d*} \\ A_4^d A_2^{d*} & A_4^d A_4^{d*} \end{bmatrix} \quad (29)$$

and

$$\mathbf{T}_{\text{dd}} = \mathbf{I} + g_{00}[1 - i\alpha\mathcal{T}_{\text{dd}}]\mathcal{T}_{\text{dd}} \quad (30)$$

with

$$\mathcal{T}_{\mathrm{dd}} = \begin{bmatrix} A_1^d A_1^{d*} & A_1^d A_3^{d*} \\ A_3^d A_1^{d*} & A_3^d A_3^{d*} \end{bmatrix}, \qquad (31)$$

returning to previous form for the amplification matrix **T**. **I** is the 2×2 identity matrix. We recall that g_{00} is the scalar gain to find at threshold and $\alpha = \frac{\partial n_r / \partial N}{\partial n_i / \partial N}$ is Henry's coefficient accounting for the relative change of the real part of the optical index (n_r) [59]. In the present form, the expression for α dealing with a satellite mode does not take into account the gain saturation by the central mode. The previous expression of α should then be changed into $\alpha \mathcal{T}_{\mathrm{uu}}$ and $\alpha \mathcal{T}_{\mathrm{dd}}$ in order to consider gain self-saturation without much computational effort.

B. Transfer and scattering matrix formalism for the anisotropic optical cavity

We are now going to tackle the issue of propagation end eigenmodes in optical cavities including active regions (QWs), barriers, host, and Bragg mirrors. One considers first a single QW as an optical source. Figure 3 displays a simple laser structure consisting of *a single active dipole layer* embedded in a multilayer system and described by its optical transfer-matrix components, $\mathbf{M}^{(1)}$ and $\mathbf{M}^{(2)}$. Those transfer matrices connect the amplitudes of the *outgoing* and *ingoing* waves from both external parts of the active layer to the *top* (1) and *bottom* (2), respectively. In that sense, the **M** matrix contains all the optical properties of the host (birefringence, strain, and optical anisotropies) from the permittivity tensor. Moreover, the **T** matrix includes information on the optical gain. More details are given in Appendix A. From (A1), (A2), and (27) we obtain a compact form of the basic equation for the calculation of the field amplitudes emitted from the structure $\mathbf{A}_{\mathrm{up}}^{(0)}$ and $\mathbf{A}_{\mathrm{down}}^{(N+1)}$ according to

$$\widetilde{\mathbf{A}}_{\mathrm{M}} \begin{bmatrix} \mathbf{A}_{\mathrm{up}}^{(0)} \\ \mathbf{A}_{\mathrm{down}}^{(N+1)} \end{bmatrix} = -\gamma \begin{bmatrix} \mathbf{A}_{\mathrm{up}}^d \\ \mathbf{A}_{\mathrm{down}}^d \end{bmatrix}, \qquad (32)$$

where

$$\widetilde{\mathbf{A}}_{\mathrm{M}} = \begin{bmatrix} -\widetilde{\mathbf{M}}_{\mathrm{uu}}^{(1)} & \mathbf{T}_{\mathrm{uu}} \mathbf{M}_{\mathrm{ud}}^{(2)} \\ \mathbf{T}_{\mathrm{dd}} \widetilde{\mathbf{M}}_{\mathrm{du}}^{(1)} & -\mathbf{M}_{\mathrm{dd}}^{(2)} \end{bmatrix}. \qquad (33)$$

The condition for a resonant eigenmode (no spontaneous emission $\gamma_{\mathrm{sp}} = 0$) is the zero determinant of the constituent matrix $\widetilde{\mathbf{A}}_{\mathrm{M}}$. In the simplest case of a laser cavity of thickness d, wave vector $k_0 = 2\pi/\lambda$, and complex refractive index $n = n_r - i n_i$, one obtains in this way the well-known condition for the resonance wavelength $k_0 d n_r = m\pi$ by finding the zero of the imaginary part of the determinant. From the zero of its real part, one obtains $g = e^{k_0 d n_i/2} - 1$, giving the condition for the optical gain g at the laser threshold. From Eq. (32), the conditions for resonance and eigenmodes for a single active layer are then generally given by

$$\mathrm{Det}[\widetilde{\mathbf{A}}_{\mathrm{M}}] = 0 \qquad (34)$$

or equivalently

$$\left[\mathbf{T}_{\mathrm{dd}} \widetilde{\mathbf{M}}_{\mathrm{du}}^{(1)} \left(\widetilde{\mathbf{M}}_{\mathrm{uu}}^{(1)} \right)^{-1} \right]^{-1} = \mathbf{T}_{\mathrm{uu}} \mathbf{M}_{\mathrm{ud}}^{(2)} \left(\mathbf{M}_{\mathrm{dd}}^{(2)} \right)^{-1}. \qquad (35)$$

However, the transfer matrix **M** described by (A1) and (A2) connecting the upper and lower field amplitudes is only suitable to describe a *single active region*. One can easily be convinced that it cannot be extended to the case of *multiple QWs*. The scattering matrix (S-matrix) formalism is much more appropriate to treat this general case. It describes the amplification and optical propagation or diffusion of the *in-going* wave-amplitudes into *outgoing* wave amplitude. For more details see Appendix B. From (B1), (B2), and (27), one derives

$$\widetilde{\mathbf{A}}_{\mathrm{S}} = \begin{bmatrix} \mathbf{S}_{\mathrm{uu}}^{(1)} & \mathbf{0} \\ \mathbf{0} & \mathbf{S}_{\mathrm{dd}}^{(2)} \end{bmatrix}^{-1} \begin{bmatrix} \mathbf{T}_{\mathrm{ud}} \mathbf{S}_{\mathrm{du}}^{(1)} - \mathbf{I} & \mathbf{T}_{\mathrm{uu}} \mathbf{S}_{\mathrm{ud}}^{(2)} \\ \mathbf{T}_{\mathrm{dd}} \mathbf{S}_{\mathrm{du}}^{(1)} & \mathbf{T}_{\mathrm{du}} \mathbf{S}_{\mathrm{ud}}^{(2)} - \mathbf{I} \end{bmatrix}, \qquad (36)$$

where **I** is the 2×2 unit matrix. The $\widetilde{\mathbf{A}}_{\mathrm{S}}$ matrix in Eq. (36) consists in a more general expression suitable for recursive calculations. **T** defined in (27) is generalized into a more general form including possible off-diagonal submatrices $\mathbf{T}_{\mathrm{ud}}$ and $\mathbf{T}_{\mathrm{du}}$ required to describe coherent multiple reflections and interference effects between two active regions (discussed in detail in the next subsection). These cannot be included in the **M**-matrix formulation and they are derived from a general recursive formula detailed hereafter. In the case where $\mathbf{T}_{\mathrm{ud}} = \mathbf{T}_{\mathrm{du}} = \mathbf{0}$ (a single active region is considered), finding the zero determinant of the $\widetilde{\mathbf{A}}_{\mathrm{M}}$ and $\widetilde{\mathbf{A}}_{\mathrm{S}}$ matrices in Eqs. (33) and (36) gives naturally equivalent results for optical modes (polarization and wavelength) and gain (threshold). The conditions for resonance and eigenmodes for multiple-QW structures are

$$\mathrm{Det}[\widetilde{\mathbf{A}}_{\mathrm{S}}] = 0 \qquad (37)$$

or equivalently

$$\mathrm{Det} \begin{bmatrix} \mathbf{T}_{\mathrm{ud}} \mathbf{S}_{\mathrm{du}}^{(1)} - \mathbf{I} & \mathbf{T}_{\mathrm{uu}} \mathbf{S}_{\mathrm{ud}}^{(2)} \\ \mathbf{T}_{\mathrm{dd}} \mathbf{S}_{\mathrm{du}}^{(1)} & \mathbf{T}_{\mathrm{du}} \mathbf{S}_{\mathrm{ud}}^{(2)} - \mathbf{I} \end{bmatrix} = 0 \qquad (38)$$

that we will consider now by implementing a general recursion method for deriving **S** and **T** tensors in the most general cases. The resonant condition can be written as

$$\left[\mathbf{T}_{\mathrm{dd}} \mathbf{S}_{\mathrm{du}}^{(1)} \left(\mathbf{T}_{\mathrm{ud}} \mathbf{S}_{\mathrm{du}}^{(1)} - \mathbf{I} \right)^{-1} \right]^{-1} = \mathbf{T}_{\mathrm{uu}} \mathbf{S}_{\mathrm{ud}}^{(2)} \left(\mathbf{T}_{\mathrm{du}} \mathbf{S}_{\mathrm{ud}}^{(2)} - \mathbf{I} \right)^{-1} \qquad (39)$$

or equivalently

$$\begin{aligned} \mathbf{T}_{\mathrm{dd}} \mathbf{S}_{\mathrm{du}}^{(1)} \left(\mathbf{T}_{\mathrm{ud}} \mathbf{S}_{\mathrm{du}}^{(1)} - \mathbf{I} \right)^{-1} \mathbf{T}_{\mathrm{uu}} \mathbf{S}_{\mathrm{ud}}^{(2)} \left(\mathbf{T}_{\mathrm{du}} \mathbf{S}_{\mathrm{ud}}^{(2)} - \mathbf{I} \right)^{-1} &= \mathbf{I}, \\ \mathbf{T}_{\mathrm{dd}} \mathbf{S}_{\mathrm{du}}^{(1)} \sum_N \left(\mathbf{T}_{\mathrm{ud}} \mathbf{S}_{\mathrm{du}}^{(1)} \right)^N \mathbf{T}_{\mathrm{uu}} \mathbf{S}_{\mathrm{ud}}^{(2)} \sum_M \left(\mathbf{T}_{\mathrm{du}} \mathbf{S}_{\mathrm{ud}}^{(2)} \right)^M &= \mathbf{I}, \end{aligned} \qquad (40)$$

giving the general phase-matching conditions for the **E** waves after all possible optical pathways (S matrix) and amplifications (T matrix) in the optical cavity. In that sense, N and M are the number of the partial back-and-forth travelings in the respective upper and down part of the cavity (see Fig. 4).

C. Recursive formulas for multiple active regions

The S-matrix scheme adopted here is suitable to describe multiple optical active zones, their optical amplification, and the propagation of the **E** wave inside the cavity. In particular, the S-matrix scheme enables us to provide a recursive formula
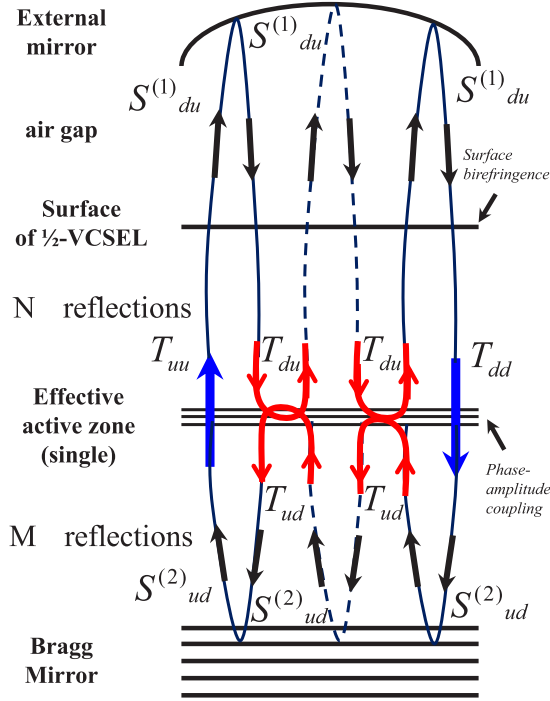
FIG. 4. Sketch of the phase matching in 1/2-VCSEL structure involving a multiple reflection, propagation, and amplification process in the optical semiconductor cavity containing one effective active layer, the properties of which are derived by recursive method. $\mathbf{S}_{du}$ and $\mathbf{S}_{ud}$ correspond to propagation and reflection effects with respective N (top) and M (bottom) reflection processes. $\mathbf{T}_{ud}$ and $\mathbf{T}_{du}$ represent reflection after amplification in the effective active zone whereas $\mathbf{T}_{uu}$ and $\mathbf{T}_{dd}$ correspond to forward amplification.

for the optical gain involving multiple dipole sources that could be implemented in numerical procedures for the derivation of optical eigenmodes of VCSELs and spin VCSELs. The result is the following. Let us consider that the dipole active layers are described by the dipole source vectors $\mathbf{A}^{(n)d}$ and $\mathbf{A}^{(n+1)d}$ and the optical gain tensors $\mathbf{T}^{(n)}$ and $\mathbf{T}^{(n+1)}$. The definitions of vectors and optical gain are similar to (27). The effective dipole layer is found by using the following relationship:

$$\begin{bmatrix} \mathbf{A}_{\text{up}}^{(n)'} \\ \mathbf{A}_{\text{down}}^{(n+1)''} \end{bmatrix} = \mathbf{T}^{(n,n+1)} \begin{bmatrix} \mathbf{A}_{\text{up}}^{(n+1)''} \\ \mathbf{A}_{\text{down}}^{(n)'} \end{bmatrix} + \mathbf{A}^{(n,n+1)d}, \quad (41)$$

where $\mathbf{T}^{(n,n+1)}$ is in the form

$$\mathbf{T}^{(n,n+1)} = \begin{bmatrix} \mathbf{T}_{uu}^{(n,n+1)} & \mathbf{T}_{ud}^{(n,n+1)} \\ \mathbf{T}_{du}^{(n,n+1)} & \mathbf{T}_{dd}^{(n,n+1)} \end{bmatrix}. \quad (42)$$

The equivalent dipole source vector, $\mathbf{A}^{(n,n+1)d}$, and optical gain tensor $\mathbf{T}^{(n,n+1)}$ of the total system are written

$$\mathbf{T}^{(n,n+1)} = \begin{bmatrix} \mathbf{0} & \mathbf{T}_{ud}^{(n)} \\ \mathbf{T}_{du}^{(n+1)} & \mathbf{0} \end{bmatrix} + \mathbf{B} \begin{bmatrix} \mathbf{T}_{uu}^{(n+1)} & \mathbf{0} \\ \mathbf{0} & \mathbf{T}_{dd}^{(n)} \end{bmatrix}, \quad (43)$$

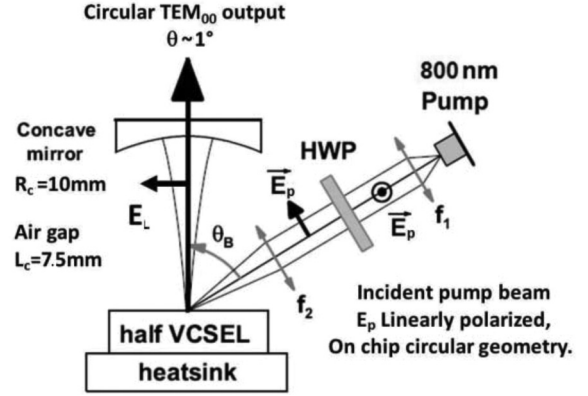$$\mathbf{A}^{(n,n+1)d} = \mathbf{A}^{(n)d} + \mathbf{B} \mathbf{A}^{(n+1)d} \quad (44)$$

FIG. 5. Sketch and geometry of the 1/2-VCSEL devices investigated in this paper showing 1/2-VCSEL structure as the gain mirror, the optical pumping system, and the stable plano-concave-type optical cavity (air gap $L_c = 7.5$ mm) [20,37,38].

where

$$\mathbf{B} = \begin{bmatrix} \mathbf{T}_{uu}^{(n)}\mathbf{S}_{uu}^{(n)} & \mathbf{T}_{uu}^{(n)}\mathbf{S}_{ud}^{(n)} \\ \mathbf{T}_{dd}^{(n+1)}\mathbf{S}_{du}^{(n)} & \mathbf{T}_{dd}^{(n+1)}\mathbf{S}_{dd}^{(n)} \end{bmatrix}$$

$$\times \begin{bmatrix} \mathbf{I} - \mathbf{T}_{ud}^{(n+1)}\mathbf{S}_{du}^{(n)} & -\mathbf{T}_{ud}^{(n+1)}\mathbf{S}_{dd}^{(n)} \\ -\mathbf{T}_{du}^{(n)}\mathbf{S}_{uu}^{(n)} & \mathbf{I} - \mathbf{T}_{du}^{(n)}\mathbf{S}_{ud}^{(n)} \end{bmatrix}^{-1}. \quad (45)$$

Note that the effective $\mathbf{T}$ matrix consists of nonzero off-diagonal submatrices $\mathbf{T}_{ud}$ and $\mathbf{T}_{du}$, describing coherent reflection processes between consecutive active regions. In Sec. IV, we will show that $\mathbf{T}_{ud}$ and $\mathbf{T}_{du}$ may largely impact the resonance conditions on the wavelength and the frequency splitting in anisotropic VCSELs. More details of the numerical recursive procedure are shown in Appendix C.

IV. EMISSION FROM 1/2-VCSEL STRUCTURES WITH LINEAR BIREFRINGENCE AND GAIN: MODEL VS EXPERIMENTS

We turn now to experiments and connect our calculation method to some real experimental 1/2-VECSEL structures for two different cavity geometries involving linear birefringences. The typical setup is displayed in Fig. 5. This section includes robust numerical predictions for eigenmodes with strong local linear birefringence and linear gain anisotropy effects. The results are compared to experimental measurements with the goal to disentangle both surface and interface anisotropies. We will consider two different sources of linear birefringence at the interface and/or in the QWs.

A. Main physical issues: From a single source to multiple recursion

It is well known that the birefringence in the laser optical cavity may induce a degeneracy lift of the optical frequencies of polarization eigenvectors, leading to a frequency splitting in the rf domain due to difference of their optical path. A simple model for the derivation of the corresponding phase or frequency splitting between two consecutive modes after one
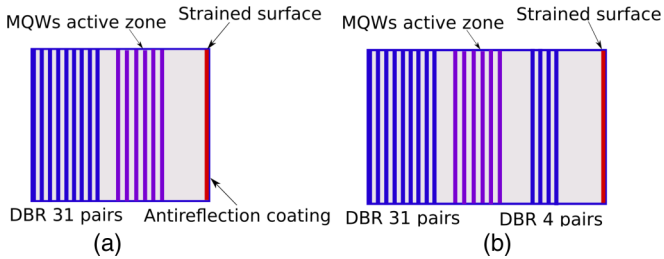
FIG. 6. Description of the 1/2-VECSEL structures under study (a) with (S1, left) and (b) without (S2, right) the moderately reflective Bragg mirror. S1 is composed of an antireflection coating at the surface.

round trip in the optical cavity of length L_c is given by [55]

$$\Delta\varphi_l = 2k_0 L_c \Delta n, \tag{46}$$

where $\Delta n = n_y - n_x$ is the modal optical index difference between the eigenvector axis (integrated over the cavity length), and k_0 is the free-space wave vector of light. The frequency splitting is given by $2\pi\Delta f = -\Delta\varphi_l \times c/2\bar{n}L_c$ where $\bar{n}$ is the average modal index.

In the nonintentionally doped GaAs-based nanostructures considered here, emitting vertically along the [001] crystal axis under optical pumping (no vertical static electric field applied), the typical sources of linear optical anisotropy, and thus birefringence, might find their origin in three characteristic regions [37]: at the Bragg interfaces, in the QW layers, and at the top air-semiconductor surface.

We will consider the latter two contributions, as the strongest. An important remark is that the effective phase-amplitude birefringence in QWs depends on the optical gain and then on the losses unlike purely electro-optic birefringence arising from the surface.

The power of the present method is to correctly include the gain properties in a self-consistent manner. For instance, we will show that restricting ourselves to the use of a simple round-trip model suppressing main interferences and inter-QW amplification [switching off $\mathbf{T}_{ud}$ and $\mathbf{T}_{du}$ in Eq. (36)] may lead to inaccuracy in the determination of the birefringence from the value of the average refractive index, Δn.

B. Modeling a real VECSEL involving linear anisotropies

1. Description of the 1/2-VCSEL structures

We consider two different structures (S1 and S2 for samples 1 and 2) [37] represented in Fig. 6, the anisotropic optical properties of which have been investigated by high-resolution microwave rf techniques [37]. In detail, the nonintentionally doped 1/2-VCSEL structure was grown by metalorganic chemical vapor deposition on a [001] GaAs substrate [19]. S1 and S2 are composed of a high reflectivity (99.9%) bottom AlAs/GaAs Bragg mirror (31.5 pairs) and a GaAs active layer of $13\lambda/2$ thickness containing six strain-balanced InGaAs/GaAsP QWs emitting at $\lambda \simeq 1\,\mu$m for S1 and $\lambda \simeq 1.06\,\mu$m for S2. Each QW is placed at an antinode of the optical standing wave, following a nonuniform longitudinal distribution ensuring uniform QW carrier excitation. This ensures a low threshold carrier density and homogeneous gain broadening as needed for single longitudinal mode operation
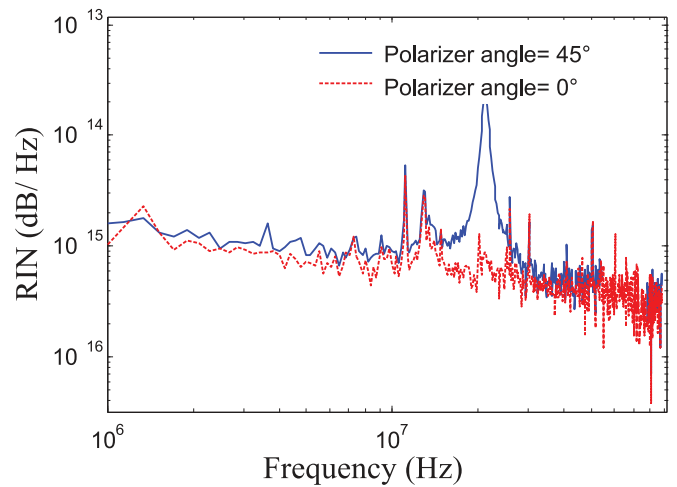

FIG. 7. Experimental birefringence measurement, via orthogonal **E**-field polarization mode beating on a low noise photodiode with a laser beam passing through a polarizer rotated at 45 deg° from the [110] axis: an example of the measured rf spectrum, obtained with sample 1 in a 7.5-mm-long cavity and a concave output coupler with $T = 0.7\%$. The absence of the peak in the red dashed curve confirms that the observed beat note is due the orthogonal polarization mode [37].

[19,20,37]. S1 is ended by a dielectric antireflection coating. S2 is ended by a moderately reflective top epitaxial AlGaAs Bragg mirror, that may affect the sensitivity of the surface and QW anisotropy. This leads to an optical confinement of the **E** wave which is strongly enhanced on the QWs. The VECSEL devices are depicted in Fig. 5. The gain structures were optically pumped in the GaAs barriers close to Brewster incidence angle θ_B, by using a linearly polarized single mode 800-nm diode, focused with a pair of aspheric lenses with the focal lengths f_1 and f_2 on a $\simeq 35$-μm spot radius with a circular in-plane geometry. The passive optical cavity is a high finesse stable planoconcave resonator of $L_c \simeq 7.5$ mm, closed by a concave output coupler ($T = 0.7\%$ for S1 and 13% for S2) of radius of curvature $R_c = 10$ mm. The minimum waist of the Gaussian beam occurs at the plan mirror. The typical fundamental TEM$_{00}$ beam waist is $w_0 \sim 37\,\mu$m here, and exhibits a circular geometry. From an experimental point of view, in contrast to the case of monolithic microcavity-VCSEL devices [24,32,38], for conventional VECSELs both the frequency splitting and the power beating between polarization eigenmodes are too small to be able to be measured using optical spectrometers. Those experiments are thus based on the mixing of the two orthogonal cavity eigenvectors (see Siegman's book for reference [55]), and on the observation of the beat note in the rf domain, by measuring on a photodiode the power spectral density of the laser total power fluctuations [37,55], as shown in Fig. 7.

2. Optical constants

The permittivity constants ε used in the calculation are the following: $\varepsilon_{\text{GaAs}}(\lambda = 1000\,\text{nm}) = 12.3$, $\varepsilon_{\text{GaAs}}(\lambda = 1060\,\text{nm}) = 12.09$, $\varepsilon_{\text{AlAs}}(\lambda = 1000\,\text{nm}) = 8.7$, $\varepsilon_{\text{AlAs}}(\lambda = 1060\,\text{nm}) = 8.63$ [73], $\varepsilon_{\text{InGaAs}}(\lambda = 1000\,\text{nm}) = 13.1$, $\varepsilon_{\text{InGaAs}}(\lambda = 1060\,\text{nm}) = 12.9$ [74], $\varepsilon_{\text{GaAsP}}(\lambda = 1000\,\text{nm}) =$
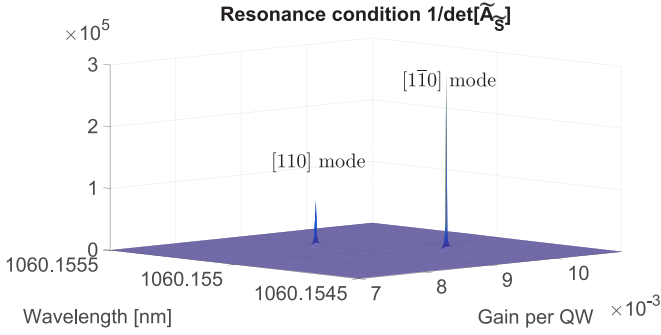
FIG. 8. Calculation of the resonance conditions of sample 2 for two linearly polarized eigenmodes oriented along the [110] and [1$\bar{1}$0] direction and $\Delta \varepsilon_s = 0.02$. Δ was taken equal to 0.95.

12.15, and $\varepsilon_{\text{GaAsP}}(\lambda = 1060 \, \text{nm}) = 11.9$ [75]. These optical constants are also in agreement with ellipsometry measurements and modeling that we have recently performed [76]. Concerning the InGaAs quantum well, we switched off the imaginary part of the optical constant being replaced by the optical gain as a controlled input parameter.

3. Detailed birefringence analysis on 1/2-VCSELs

We are going now to apply our numerical method to three different physical situations of (a) a linear birefringence at the surface only, (b) an intrinsic linear birefringence in QWs, and (c) a linear birefringence at the surface and phase-amplitude coupling in QWs.

Case a. Via a step-by-step mesh-calculation procedure on both the wavelength λ and optical gain g_{00} parameter, resonances and eigenmodes for the S2 structure are highlighted, from Eq. (38), by pointing to the peaked maxima of $1/\det[\widetilde{\mathbf{A}}_S]$. Under these conditions, one finds a comb of resonance doublets, as expected, the two representatives of which are plotted in Fig. 8. The linear gain dichroism has been fixed at $\Delta = 0.95$ in the present example and the linear birefringence at the surface $\Delta \varepsilon_s = (\varepsilon_{x'x'} - \varepsilon_{y'y'})/2 = 0.02$, where $\varepsilon_{x'x'}$ and $\varepsilon_{y'y'}$ are the permittivity tensor components of a surface layer along the directions parallel to [110] and [1$\bar{1}$0], respectively, as depicted in Fig. 1. The thickness of the birefringent surface layer has been fixed to 50 nm. The analysis of the eigenmode polarization demonstrates an orientation of the **E** wave along respective [110] and [1$\bar{1}$0] directions for the whole doublets. One can note that the two consecutive peaks occur at two different frequencies as expected from the linear birefringence and moreover occur for two different calculated amplitude gains, respectively, 0.85 and 0.95% per quantum well for loss compensation and corresponding to external mirror transmission of about 13% on the electromagnetic wave intensity (6× QWs ×2 on the intensity gain). The relative difference of the gain of about 10% is then representative differential gain $(1 - \Delta^2)$ chosen for this particular example.

Case b. Figure 9(a) displays the frequency splitting between two consecutive longitudinal modes with and without linear birefringence $\Delta \varepsilon_{\text{QW}}$ in the QWs introduced as an adjustable parameter for a total thickness of 48 nm (for six quantum wells, 8 nm each). Canceling all the birefringence $\Delta \varepsilon = 0$,
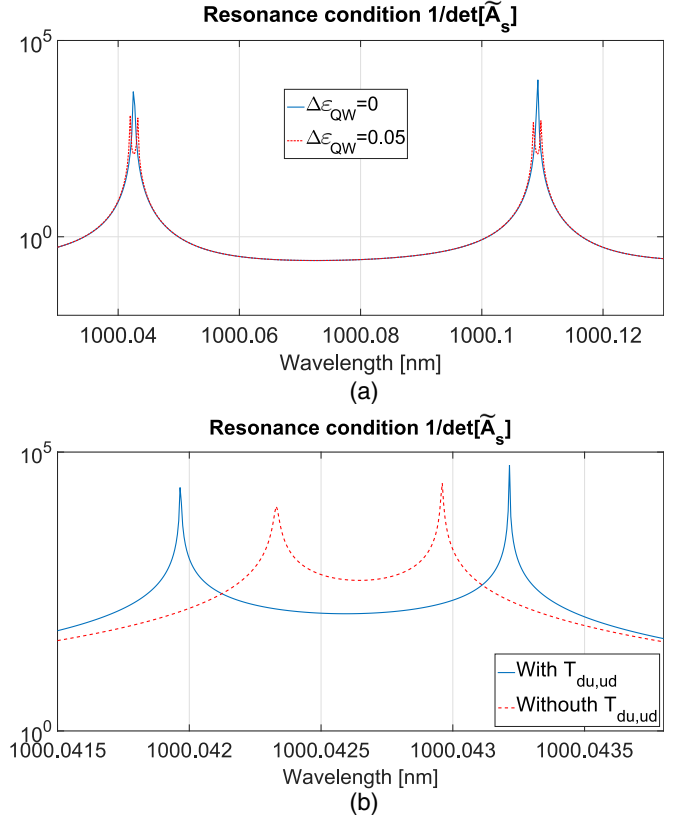

(a)

(b)

FIG. 9. (a) Calculation of multimode emission and mode splitting for $\Delta \varepsilon_{\text{QW}} = 0$ (solid blue line) and $\Delta \varepsilon_{\text{QW}} = 0.05$ (dashed red line with peak doublets) inside the QW of sample 1. (b) Calculation of mode splitting inside the QW of sample 1. The solid blue curve ($\Delta f = 359 \, \text{MHz}$) and the dashed red curve ($\Delta f = 195 \, \text{MHz}$) describe the resonance conditions for models with and without off-diagonal elements $\mathbf{T}_{\text{du}}$ and $\mathbf{T}_{\text{ud}}$, respectively.

the frequency splitting between longitudinal modes $\Delta f = 19.2 \, \text{GHz}$ matches pretty well the value $\Delta f = c/2t_{\text{air}} = 20 \, \text{GHz}$ expected from the calculation of the phase matching in a simple air external cavity of thickness t_{air}. The long extension of the air cavity compared to the semiconductor part makes it so that the optical phase develops preferentially in that region.

Figure 9(b) shows the details of the two transverse modes from the ones calculated in Fig. 9(a). Note that switching off any inter-QW amplification processes (by switching off the off-diagonal elements $\mathbf{T}_{\text{du}}$ and $\mathbf{T}_{\text{ud}}$) leads to a certain inaccuracy of the mode splitting Δf in the megahertz range for 1/2-cavity VCSELs. Switching on $\mathbf{T}_{\text{du}}$ and $\mathbf{T}_{\text{ud}}$ off-diagonal components appears then mandatory for a correct determination of the layer-selected anisotropic optical constant Δn (permittivity tensor $\Delta \varepsilon$).

Case c. We now proceed to the investigation of eigenmodes including linear gain anisotropy as relaxed parameters with phase-amplitude correlation (Henry's factor). We do not consider any other linear birefringence $\Delta \varepsilon_{\text{QW}}$ than the phase-amplitude coupling. This section refers to the recent work of Ref. [37] giving opposite sign of the frequency splitting $\Delta f = -16.5$ and $+69$ MHz for S1 and S2 as shown in Table I. Here, Δf is counted positive when $f_{[110]} > f_{[1\bar{1}0]}$ according to our convention. The two-dimensional maps

TABLE I. Measured polarization mode beat frequency Δf_b [37], extracted anisotropic parameters $\Delta \varepsilon_{s,1,2}$ for experimentally obtained $\Delta = \Delta_1 = \Delta_2 = 0.95$, and anisotropic parameters $\Delta \varepsilon_s = \Delta \varepsilon_{s,1} = \Delta \varepsilon_{s,2}$ together with $\Delta = 0.82$.

	Sample 1	Sample 2
Δf_b	-16.5 MHz	$+69$ MHz
$\Delta \varepsilon_{s,1,2}$ ($\Delta = 0.95$)	$+0.0152$	-0.0245
$\Delta \varepsilon_s$ ($\Delta = 0.82$)	$+0.02$	

presented in Figs. 10(a) (S1 sample) and 10(b) (S2 sample) display the particular dependence of the frequency splitting, Δf, between the two orthogonal linear polarizations for the two 1/2-VCSELs vs the gain anisotropy parameter Δ and an additional surface linear birefringence ($\Delta \varepsilon_s$) with an effective surface thickness of 50 nm. In these examples, we fix the value of $\alpha = 3$ [37]. The two linear polarizations are, respectively, found along [110] and [1$\bar{1}$0] directions with inverted frequency splitting between samples 1 and 2. One observes separately the dependence of Δf on Δ for fixed $\Delta \varepsilon_s$ (lines from left to right) and the dependence of Δf on the linear gain anisotropy Δ on the horizontal axis. Simple linear parametrization resulting from our calculation gives a phenomenological dependence of Δf [MHz] on $\Delta \varepsilon_s$ and Δ for both samples as

$$\Delta f_1 [\text{MHz}] = -1220 \Delta \varepsilon_{s,1} + 40(1 - \Delta_1), \qquad (47)$$

$$\Delta f_2 [\text{MHz}] = -1700 \Delta \varepsilon_{s,2} + 550(1 - \Delta_2). \qquad (48)$$
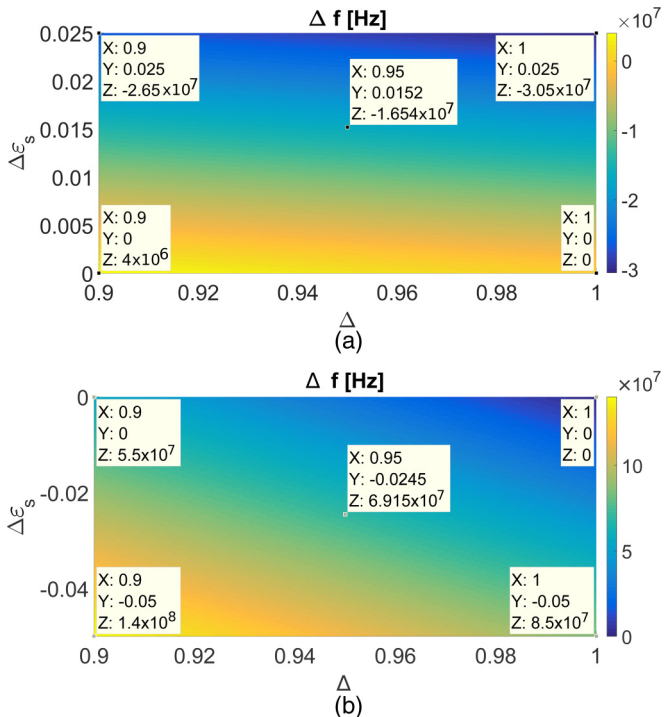

FIG. 10. Dependence of Δf between two orthogonal linear polarizations on anisotropic parameters of QWs $\Delta \varepsilon_{\text{QW}}$ and surface $\Delta \varepsilon_s$ of (a) S1 and (b) S2.

The sensitivity of Δf_2 (S2) on the linear gain dichroism Δ_2 is more than a factor of 13 larger than that of S1. This finding describes the microresonance effect in the region of QWs combined with a larger carrier optical pumping due to the particularly high decay rate of the cavity. On the other hand, the birefringence at the surface, delocalized from the optical confinement region, gives about the same equivalent effect on the frequency mode splitting for the two samples. If one assumes that the two samples are characterized by an identical surface strain and birefringence $\Delta \varepsilon_s = \Delta \varepsilon_{s,1} = \Delta \varepsilon_{s,2}$, and identical active zones (same linear gain dichroism $\Delta = \Delta_1 = \Delta_2$), the common solution of the above equations gives $\Delta \varepsilon_s = +0.02$ and $\Delta = 0.82$. The change of the sign of the frequency splitting between S1 and S2 may then be understood as (1) an opposite effect of the linear birefringence between surface and active layers together with (2) a main contribution from the surface for S1 due to small optical losses and gain, and small optical confinement, and (3) an enhanced contribution of linear birefringence of QWs for S2 due to larger optical losses and gain together with a strong optical confinement.

The matching of the frequency splitting to the experimental situation under the assumption of the same linear gain dichroism of $\Delta = 0.95$ (linear gain dichroism of 10% on the intensity) for samples S1 and S2 gives a surface strain birefringence $\Delta \varepsilon_{s,1}$ of opposite sign of the order of $+0.015$ for S1 and $\Delta \varepsilon_{s,2} = -0.025$ for S2. QW gain dichroism of about 10–30% has been measured in Refs. [19,37]. On the other hand, a surface birefringence with opposite sign between S1 and S2 would be surprising from a technological and physical point of view.

V. CONCLUSIONS

The mathematical approach presented in this paper offers a powerful method for modeling of the laser eigenmodes of VCSELs and spin VCSELs with local linear birefringence and linear gain dichroism caused by symmetry reduction on the III-V semiconductor interfaces, surface reconstruction, and strain effects. The present paper has revealed the important role of the different local birefringences in the eigenmodes and frequency splitting together with the need to correctly describe optical amplification. Recursive formulas used for calculation of the effective active region enable us to include the interference and reflection effects between both active regions together with amplification of multiple reflected light inside the MQW region. Together with experimental measurement, it can be used to disentangle anisotropic optical constants in the realistic VCSELs and VECSELs from different depths of the structure as it has been shown for the surface and the QWs. The present method can be advantageously used in the future to derive general properties of single and coupled modes (dynamics) of VCSELs and 1/2-VECSELs involving linear anisotropies. Moreover, on the grounds of very recent experiments [18], the approach developed in this paper can be used to extract the eigenmode properties (polarization, threshold, and mode splitting) of semiconductor spin lasers under circular-polarized pumps and local linear birefringence.

APPENDIX A: THE 4 × 4 TRANSFER-MATRIX FORMALISM

Figure 3 shows the modeled structure consisting of an active dipole layer surrounded by a multilayer system described by the transfer matrices $\mathbf{M}^{(1)}$ and $\mathbf{M}^{(2)}$. The matrices relate the amplitudes of the waves propagating from and toward the system

$$\begin{bmatrix} \mathbf{A}''_{\text{up}} \\ \mathbf{A}''_{\text{down}} \end{bmatrix} = \begin{bmatrix} \mathbf{M}^{(2)}_{\text{uu}} & \mathbf{M}^{(2)}_{\text{ud}} \\ \mathbf{M}^{(2)}_{\text{du}} & \mathbf{M}^{(2)}_{\text{dd}} \end{bmatrix} \begin{bmatrix} \mathbf{A}^{(N+1)}_{\text{up}} \\ \mathbf{A}^{(N+1)}_{\text{down}} \end{bmatrix}, \quad \text{(A1)}$$

$$\begin{bmatrix} \mathbf{A}^{(0)}_{\text{up}} \\ \mathbf{A}^{(0)}_{\text{down}} \end{bmatrix} = \begin{bmatrix} \mathbf{M}^{(1)}_{\text{uu}} & \mathbf{M}^{(1)}_{\text{ud}} \\ \mathbf{M}^{(1)}_{\text{du}} & \mathbf{M}^{(1)}_{\text{dd}} \end{bmatrix} \begin{bmatrix} \mathbf{A}'_{\text{up}} \\ \mathbf{A}'_{\text{down}} \end{bmatrix}, \quad \text{(A2)}$$

and from (A2) one can obtain by matrix inversion

$$\begin{bmatrix} \mathbf{A}'_{\text{up}} \\ \mathbf{A}'_{\text{down}} \end{bmatrix} = \begin{bmatrix} \widetilde{\mathbf{M}}^{(1)}_{\text{uu}} & \widetilde{\mathbf{M}}^{(1)}_{\text{ud}} \\ \widetilde{\mathbf{M}}^{(1)}_{\text{du}} & \widetilde{\mathbf{M}}^{(1)}_{\text{dd}} \end{bmatrix} \begin{bmatrix} \mathbf{A}^{(0)}_{\text{up}} \\ \mathbf{A}^{(0)}_{\text{down}} \end{bmatrix}, \quad \text{(A3)}$$

where $\mathbf{A}^{(0)}$ and $\mathbf{A}^{(N+1)}$ describe the amplitudes in the superstrate and substrate. Similarly, $\mathbf{A}'$ and $\mathbf{A}''$ are the amplitudes above and below the active dipole layer. Note that four waves propagate in each layer of the system. Therefore, the amplitudes in (A1) and (A2) represent the amplitude vectors corresponding to two orthogonal polarizations, for example, $\mathbf{A}^{(0)}_{\text{down}} = [A^{(0)}_1; \ A^{(0)}_3]^T$ and $\mathbf{A}^{(0)}_{\text{up}} = [A^{(0)}_2; \ A^{(0)}_4]^T$. The submatrices in (A1) and (A2) are 2×2 matrices and the tilde denotes the blocks of the inverse matrix $\widetilde{\mathbf{M}}^{(1)} = [\mathbf{M}^{(1)}]^{-1}$. Note that in the case of lasers the light is only emitted from the structure: $\mathbf{A}^{(0)}_{\text{down}} = \mathbf{A}^{(N+1)}_{\text{up}} = \mathbf{0}$. Equations (A1) and (A2) are compactly written as the 4×4 matrix equations (1) and (2) from Ref. [53].

From (A1), (A2), and (27) we obtain a compact form of the basic equation (32) for the field emitted from the structure, which is used to calculate the amplitudes of the field emitted from the structure $\mathbf{A}^{(0)}_{\text{up}}$ and $\mathbf{A}^{(N+1)}_{\text{down}}$ from the dipole source vectors $\mathbf{A}^d_{\text{up}}$ and $\mathbf{A}^d_{\text{down}}$. Equations (29), (31), and (32) are the compactly written 4×4 matrix equations (8)–(10) in Ref. [53].

APPENDIX B: SCATTERING MATRIX FORMALISM

While the transfer matrix $\mathbf{M}$ described by Eqs. (A1) and (A2) relates the upper and lower field amplitudes, the scattering matrix (S-matrix) is defined using the amplitudes of the waves incoming toward and outgoing from the structure. Let us consider a similar structure as before shown in Fig. 11, in which the active dipole layer is surrounded by the multilayer subsystems described using the scattering matrices $\mathbf{S}^{(1)}$ and $\mathbf{S}^{(2)}$. The amplitudes of the waves are related using the matrix formulas

$$\begin{bmatrix} \mathbf{A}^{(0)}_{\text{up}} \\ \mathbf{A}'_{\text{down}} \end{bmatrix} = \begin{bmatrix} \mathbf{S}^{(1)}_{\text{uu}} & \mathbf{S}^{(1)}_{\text{ud}} \\ \mathbf{S}^{(1)}_{\text{du}} & \mathbf{S}^{(1)}_{\text{dd}} \end{bmatrix} \begin{bmatrix} \mathbf{A}'_{\text{up}} \\ \mathbf{A}^{(0)}_{\text{down}} \end{bmatrix} = \mathbf{S}^{(1)} \begin{bmatrix} \mathbf{A}'_{\text{up}} \\ \mathbf{A}^{(0)}_{\text{down}} \end{bmatrix} \quad \text{(B1)}$$

and

$$\begin{bmatrix} \mathbf{A}''_{\text{up}} \\ \mathbf{A}^{(N+1)}_{\text{down}} \end{bmatrix} = \begin{bmatrix} \mathbf{S}^{(2)}_{\text{uu}} & \mathbf{S}^{(2)}_{\text{ud}} \\ \mathbf{S}^{(2)}_{\text{du}} & \mathbf{S}^{(2)}_{\text{dd}} \end{bmatrix} \begin{bmatrix} \mathbf{A}^{(N+1)}_{\text{up}} \\ \mathbf{A}''_{\text{down}} \end{bmatrix} = \mathbf{S}^{(1)} \begin{bmatrix} \mathbf{A}^{(N+1)}_{\text{up}} \\ \mathbf{A}''_{\text{down}} \end{bmatrix}. \quad \text{(B2)}$$

If we expect that light is only emitted from the structure, then $\mathbf{A}^{(0)}_{\text{down}} = \mathbf{A}^{(N+1)}_{\text{up}} = \mathbf{0}$. From (B1), (B2), and (27) we obtain the basic equation (32) for the field emitted from the structure with the matrix $\widetilde{\mathbf{A}}_S$ in Eq. (36) which consists of a more general expression suitable for the recurrent calculation.

APPENDIX C: RECURSIVE CALCULATION OF THE EFFECTIVE GAIN TENSOR

The S-matrix approach enables us to describe optical amplification, propagation, as well as interferences in multiple QW structure. The recursive S-matrix method we propose here provides a numerical solution scheme to describe any type of multilayered structures. Figure 11 schematically shows the structure including two active dipole layers, respectively, (n) and $(n+1)$, the latter being the new one to add by recursion. The composite of the two can be substituted by a single effective active dipole layer described on its own by a single effective matrix $\mathbf{T}^{(n,n+1)}_{uu,ud,du,dd}$ and single effective dipole vector $\mathbf{A}^{(n,n+1)d}$ according to the following description. Let us consider that the dipole active layers are described by the dipole source vectors $\mathbf{A}^{(n)d}$ and $\mathbf{A}^{(n+1)d}$ and the optical gain tensors $\mathbf{T}^{(n)}$ and $\mathbf{T}^{(n+1)}$. The definitions of vectors and optical
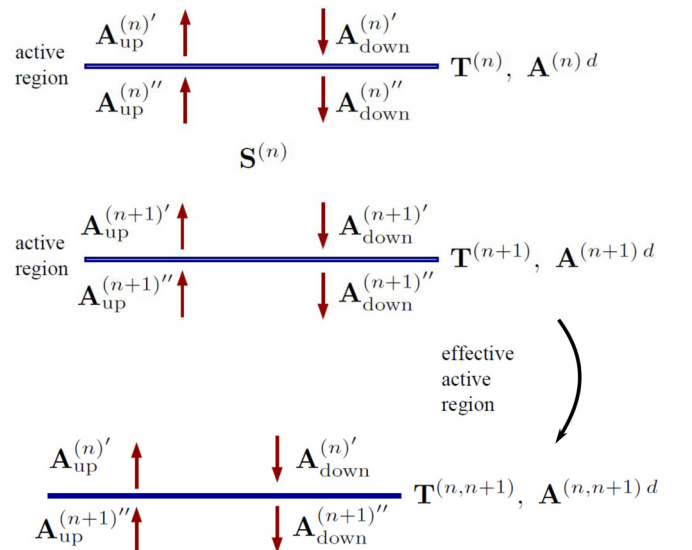

FIG. 11. Schematic description of the application of the recursive formula.

gain are similar to (27). The effective dipole layer is found by using Eqs. (41) and (42), where the effective dipole source vector $\mathbf{A}^{(n,n+1)d}$ and the effective optical gain tensor $\mathbf{T}^{(n,n+1)}$ appear in the most general case in the following form:

$$\mathbf{T}^{(n,n+1)} = \begin{bmatrix} \mathbf{0} & \mathbf{T}_{ud}^{(n)} \\ \mathbf{T}_{du}^{(n+1)} & \mathbf{0} \end{bmatrix} + \mathbf{B} \begin{bmatrix} \mathbf{T}_{uu}^{(n+1)} & \mathbf{0} \\ \mathbf{0} & \mathbf{T}_{dd}^{(n)} \end{bmatrix}, \quad \text{(C1)}$$

$$\mathbf{A}^{(n,n+1)d} = \mathbf{A}^{(n)d} + \mathbf{B}\,\mathbf{A}^{(n+1)d}, \quad \text{(C2)}$$

where

$$\mathbf{B} = \begin{bmatrix} \mathbf{T}_{uu}^{(n)}\mathbf{S}_{uu}^{(n)} & \mathbf{T}_{uu}^{(n)}\mathbf{S}_{ud}^{(n)} \\ \mathbf{T}_{dd}^{(n+1)}\mathbf{S}_{du}^{(n)} & \mathbf{T}_{dd}^{(n+1)}\mathbf{S}_{dd}^{(n)} \end{bmatrix}$$
$$\times \begin{bmatrix} \mathbf{I} - \mathbf{T}_{ud}^{(n+1)}\mathbf{S}_{du}^{(n)} & -\mathbf{T}_{ud}^{(n+1)}\mathbf{S}_{dd}^{(n)} \\ -\mathbf{T}_{du}^{(n)}\mathbf{S}_{uu}^{(n)} & \mathbf{I} - \mathbf{T}_{du}^{(n)}\mathbf{S}_{ud}^{(n)} \end{bmatrix}^{-1}. \quad \text{(C3)}$$

The effective $\mathbf{T}$ matrix consists of nonzero off-diagonal submatrices $\mathbf{T}_{ud}$ and $\mathbf{T}_{du}$, originating from the interference and reflection processes between consecutive active regions. Note that the single active layer $(n+1)$ added in the recursion procedure does not admit any off-diagonal component $\mathbf{T}_{ud}^{(n+1)} = \mathbf{0}$ and $\mathbf{T}_{du}^{(n+1)} = \mathbf{0}$ because of no internal multiple reflections. Let us demonstrate the recursive calculation for the case of three dipolar layers ($\tilde{n} = 1,2,3$) described by the block-diagonal matrix

$$\mathbf{T}^{(\tilde{n})} = \begin{bmatrix} \mathbf{T}_{uu}^{(\tilde{n})} & \mathbf{0} \\ \mathbf{0} & \mathbf{T}_{dd}^{(\tilde{n})} \end{bmatrix}, \quad \text{(C4)}$$

while the optical interactions between first and second, and second and third, dipole layers are characterized by the scattering matrices $\mathbf{S}^{(1)}$ and $\mathbf{S}^{(2)}$, respectively. In the *first step*

we calculate the effective dipole layer for the first two active regions, $n = 1$: $\mathbf{T}^{(n,n+1)} = \mathbf{T}^{(1,2)}$. According to Eqs. (43)–(45), the recursion formula gives for the gain tensor components

$$\mathbf{T}_{uu}^{(n,n+1)} = \mathbf{T}_{uu}^{(1,2)} = \mathbf{T}_{uu}^{(1)}\mathbf{S}_{uu}^{(1)}\mathbf{T}_{uu}^{(2)}, \quad \text{(C5)}$$

$$\mathbf{T}_{ud}^{(n,n+1)} = \mathbf{T}_{ud}^{(1,2)} = \mathbf{T}_{uu}^{(1)}\mathbf{S}_{ud}^{(1)}\mathbf{T}_{dd}^{(1)}, \quad \text{(C6)}$$

$$\mathbf{T}_{du}^{(n,n+1)} = \mathbf{T}_{du}^{(1,2)} = \mathbf{T}_{dd}^{(2)}\mathbf{S}_{dd}^{(1)}\mathbf{T}_{uu}^{(2)} + \mathbf{T}_{dd}^{(2)}\mathbf{S}_{du}^{(1)}, \quad \text{(C7)}$$

$$\mathbf{T}_{dd}^{(n,n+1)} = \mathbf{T}_{dd}^{(1,2)} = \mathbf{T}_{dd}^{(2)}\mathbf{S}_{dd}^{(1)}\mathbf{T}_{dd}^{(1)}, \quad \text{(C8)}$$

where new off-diagonal components $\mathbf{T}_{ud,du}^{(1,2)}$ describe coherent multiple reflections and interference effects between active regions (1) and (2). In the *second step* of the numerical procedure, we set $\mathbf{T}^{(2)} \equiv \mathbf{T}^{(1,2)}$ followed by the *third step*, when we calculate the complete effective gain tensor for $n = 2$: $\mathbf{T} = \mathbf{T}^{(2,3)}$ according to

$$\mathbf{T}_{uu}^{(2,3)} = \mathbf{T}_{uu}^{(2)}\frac{1}{\mathbf{I} - \mathbf{S}_{ud}^{(2)}\mathbf{T}_{du}^{(2)}}\mathbf{S}_{uu}^{(2)}\mathbf{T}_{uu}^{(3)}, \quad \text{(C9)}$$

$$\mathbf{T}_{ud}^{(2,3)} = \mathbf{T}_{ud}^{(2)} + \mathbf{T}_{uu}^{(2)}\mathbf{S}_{ud}^{(2)}\frac{1}{\mathbf{I} - \mathbf{T}_{du}^{(2)}\mathbf{S}_{ud}^{(2)}}\mathbf{T}_{dd}^{(2)}, \quad \text{(C10)}$$

$$\mathbf{T}_{du}^{(2,3)} = \mathbf{T}_{dd}^{(3)}\mathbf{S}_{dd}^{(2)}\frac{1}{\mathbf{I} - \mathbf{T}_{du}^{(2)}\mathbf{S}_{ud}^{(2)}\mathbf{T}_{du}^{(2)}\mathbf{S}_{uu}^{(2)}}\mathbf{T}_{uu}^{(3)} + \mathbf{T}_{dd}^{(3)}\mathbf{S}_{du}^{(2)}, \quad \text{(C11)}$$

$$\mathbf{T}_{dd}^{(2,3)} = \mathbf{T}_{dd}^{(3)}\mathbf{S}_{dd}^{(2)}\frac{1}{\mathbf{I} - \mathbf{T}_{du}^{(2)}\mathbf{S}_{ud}^{(2)}}\mathbf{T}_{dd}^{(2)}. \quad \text{(C12)}$$

The present recursive approach can be applied for an arbitrary number of active source layers and arbitrary structures. It can be thus applied for the calculation of the effective gain tensor of any complex light-emitting multilayer structures such as VCSELs and spin-VCSELs.

[1] N. C. Gerhardt and M. R. Hofmann, Spin-controlled vertical-cavity surface-emitting lasers, Adv. Opt. Techno. **2012**, 268949 (2012).

[2] H. Dery, Y. Song, P. Li, and I. Zutic, Silicon spin communication, Appl. Phys. Lett. **99**, 082502 (2011).

[3] J. Lee, W. Falls, R. Oszwaldowski, and I. Zutic, Spin modulation in semiconductor lasers, Appl. Phys. Lett. **97**, 041116 (2010).

[4] N. C. Gerhardt, M. Y. Li, H. Jähme, H. Höpfner, T. Ackemann, and M. R. Hofmann, Ultrafast spin-induced polarization oscillations with tunable lifetime in vertical-cavity surface-emitting lasers, Appl. Phys. Lett. **99**, 151107 (2011).

[5] H. Ando, T. Sogawa, and H. Gotoh, Photon-spin controlled lasing oscillation in surface-emitting lasers, Appl. Phys. Lett. **73**, 566 (1998).

[6] M. Holub, J. Shin, D. Saha, and P. Bhattacharya, Electrical Spin Injection and Threshold Reduction in a Semiconductor Laser, Phys. Rev. Lett. **98**, 146603 (2007).

[7] J. Rudolph, S. Döhrmann, D. Hägele, M. Oestreich, and W. Stolz, Room-temperature threshold reduction in vertical-cavity surface-emitting lasers by injection of spin-polarized electrons, Appl. Phys. Lett. **87**, 241117 (2005).

[8] M. Holub and B. T. Jonker, Threshold current reduction in spin-polarized lasers: Role of strain and valence-band mixing, Phys. Rev. B **83**, 125309 (2011).

[9] J. Rudolph, D. Hägele, H. M. Gibbs, G. Khitrova, and M. Oestreich, Laser threshold reduction in a spintronic device, Appl. Phys. Lett. **82**, 4516 (2003).

[10] D. Basu, D. Saha, C. C. Wu, M. Holub, Z. Mi, and P. Bhattacharya, Electrically injected InAs/GaAs quantum dot spin laser operating at 200K, Appl. Phys. Lett. **92**, 091119 (2008).

[11] I. Vurgaftman, M. Holub, B. T. Jonker, and J. R. Meyer, Estimating threshold reduction for spin-injected semiconductor lasers, Appl. Phys. Lett. **93**, 031102 (2008).

[12] C. Gothgen, R. Oszwaldowski, A. Petrou, and I. Zutic, Analytical model of spin-polarized semiconductor lasers, Appl. Phys. Lett. **93**, 042513 (2008).

[13] N. Gerhardt, S. Hovel, M. Hofmann, J. Yang, D. Reuter, and A. Wieck, Enhancement of spin information with vertical cavity surface emitting lasers, Electron. Lett. **42**, 88 (2006).

[14] S. Iba, S. Koh, K. Ikeda, and H. Kawaguchi, Room temperature circularly polarized lasing in an optically spin injected vertical-cavity surface-emitting laser with (110) GaAs quantum wells, Appl. Phys. Lett. **98**, 081113 (2011).

[15] K. Schires, R. A. Seyab, A. Hurtado, V.-M. Korpijärvi, M. Guina, I. D. Henning, and M. J. Adams, Optically-pumped dilute nitride spin-VCSEL, Opt. Express **20**, 3550 (2012).

[16] D. Basu, D. Saha, and P. Bhattacharya, Optical Polarization Modulation and Gain Anisotropy in an Electrically Injected Spin Laser, Phys. Rev. Lett. **102**, 093904 (2009).

[17] S. Hovel, N. Gerhardt, M. Hofmann, J. Yang, D. Reuter, and A. Wieck, Spin controlled optically pumped vertical cavity surface emitting laser, Electron. Lett. **41**, 251 (2005).

[18] A. Joly, G. Baili, M. Alouini, J.-M. George, I. Sagnes, G. Pillet, and D. Dolfi, Compensation of the residual linear anisotropy of phase in a vertical-external-cavity-surface-emitting laser for spin injection, Opt. Lett. **42**, 651 (2017).

[19] A. Laurain, M. Myara, G. Beaudoin, I. Sagnes, and A. Garnache, Multiwatt-power highly-coherent compact single-frequency tunable vertical-external-cavity surface-emitting semiconductor laser, Opt. Express **18**, 14627 (2010).

[20] A. Garnache, A. Ouvrard, and D. Romanini, Single-frequency operation of external-cavity VCSELs: Non-linear multimode temporal dynamics and quantum limit, Opt. Express **15**, 9403 (2007).

[21] P. Zory, *Quantum Well Lasers*, Optics and Photonics (Academic Press, New York, 1993).

[22] M. Travagnin, M. P. van Exter, A. K. Jansen van Doorn, and J. P. Woerdman, Role of optical anisotropies in the polarization properties of surface-emitting semiconductor lasers, Phys. Rev. A **54**, 1647(E) (1996); **55**, 4641(E) (1997).

[23] M. P. van Exter, M. B. Willemsen, and J. P. Woerdman, Polarization fluctuations in vertical-cavity semiconductor lasers, Phys. Rev. A **58**, 4191 (1998).

[24] M. Sondermann, M. Weinkath, and T. Ackemann, Polarization switching to the gain disfavored mode in vertical-cavity surface-emitting lasers, IEEE J. Quantum Electron. **40**, 97 (2004).

[25] M. San Miguel, Q. Feng, and J. V. Moloney, Light-polarization dynamics in surface-emitting semiconductor lasers, Phys. Rev. A **52**, 1728 (1995).

[26] M. B. Willemsen, M. P. van Exter, and J. P. Woerdman, Anatomy of a Polarization Switch of a Vertical-Cavity Semiconductor Laser, Phys. Rev. Lett. **84**, 4337 (2000).

[27] E. L. Blansett, M. G. Raymer, G. Khitrova, H. M. Gibbs, D. K. Serkland, A. A. Allerman, and K. M. Geib, Ultrafast polarization dynamics and noise in pulsed vertical-cavity surface-emitting lasers, Opt. Express **9**, 312 (2001).

[28] T. Ackemann and M. Sondermann, Characteristics of polarization switching from the low to the high frequency mode in vertical-cavity surface-emitting lasers, Appl. Phys. Lett. **78**, 3574 (2001).

[29] M. Holub, J. Shin, S. Chakrabarti, and P. Bhattacharya, Electrically injected spin-polarized vertical-cavity surface-emitting lasers, Appl. Phys. Lett. **87**, 091108 (2005).

[30] D. Hägele and M. Oestreich, Comment on electrically injected spin-polarized vertical-cavity surface-emitting lasers, Appl. Phys. Lett. **88**, 056101 (2006).

[31] M. Y. Li, H. Jähme, H. Soldat, N. C. Gerhardt, M. R. Hofmann, and T. Ackemann, Birefringence controlled room-temperature picosecond spin dynamics close to the threshold of vertical-cavity surface-emitting laser devices, Appl. Phys. Lett. **97**, 191114 (2010).

[32] A. Gahl, S. Balle, and M. San Miguel, Polarization dynamics of optically pumped VCSELS, IEEE J. Quantum Electron. **35**, 342 (1999).

[33] A. Cerjan, Y. Chong, L. Ge, and A. D. Stone, Steady-state ab initio laser theory for n-level lasers, Opt. Express **20**, 474 (2012).

[34] A. Cerjan, Y. D. Chong, and A. D. Stone, Steady-state ab initio laser theory for complex gain media, Opt. Express **23**, 6455 (2015).

[35] J.-L. Yu, Y.-H. Chen, C.-G. Tang, C. Jiang, and X.-L. Ye, Observation of strong anisotropic forbidden transitions in (001) InGaAs/GaAs single-quantum well by reflectance-difference spectroscopy and its behavior under uniaxial strain, Nanoscale Res. Lett. **6**, 210 (2011).

[36] J. Frougier, G. Baili, I. Sagnes, D. Dolfi, J.-M. George, and M. Alouini, Accurate measurement of the residual birefringence in VECSEL: Towards understanding of the polarization behavior under spin-polarized pumping, Opt. Express **23**, 9573 (2015).

[37] M. Seghilani, Highly coherent iii-v-semiconductor laser emitting phase-, amplitude- and polarization-structured light for advanced sensing applications: Vortex, spin, feedback dynamics, Ph.D. thesis, University of Montpellier, 2016.

[38] A. Garnache, A. Ouvrard, L. Cerutti, D. Barat, A. Vicet, F. Genty, Y. Rouillard, D. Romanini, and E. A. Cerda-Mendez, 2–2.7 μm single frequency tunable sb-based lasers operating in CW at RT: Microcavity and external cavity VCSELs, dfb, Proc. SPIE **6184**, 61840N (2006).

[39] F. Bretenaker and A. Le Floch, Laser eigenstates in the framework of a spatially generalized jones matrix formalism, JOSA B **8**, 230 (1991).

[40] G. Baili, L. Morvan, M. Alouini, D. Dolfi, F. Bretenaker, I. Sagnes, and A. Garnache, Experimental demonstration of a tunable dual-frequency semiconductor laser free of relaxation oscillations, Opt. Lett. **34**, 3421 (2009).

[41] S. De, A. E. Amili, G. Pillet, G. Baili, I. Sagnes, M. Alouini, and F. Bretenaker, Phase noise of the radio frequency beatnote generated by a dual frequency VECSEL, in *Proceedings of the IEEE International Topical Meeting on Microwave Photonics (MWP), 2013* (IEEE, Piscataway, NJ, 2013).

[42] S. De, A. E. Amili, I. Fsaifes, G. Pillet, G. Baili, F. Goldfarb, M. Alouini, I. Sagnes, and F. Bretenaker, Phase noise of the radio frequency (rf) beatnote generated by a dual-frequency vecsel, J. Lightwave Technol. **32**, 1307 (2014).

[43] S. De, G. Baili, M. Alouini, J.-C. Harmand, S. Bouchoule, and F. Bretenaker, Class-a dual-frequency VECSEL at telecom wavelength, Opt. Lett. **39**, 5586 (2014).

[44] S. De, G. Baili, S. Bouchoule, M. Alouini, and F. Bretenaker, Intensity-and phase-noise correlations in a dual-frequency vertical-external-cavity surface-emitting laser operating at telecom wavelength, Phys. Rev. A **91**, 053828 (2015).

[45] H. Fu and H. Haken, Multifrequency operations in a short-cavity standing-wave laser, Phys. Rev. A **43**, 2446 (1991).

[46] H. E. Türeci, A. D. Stone, and B. Collier, Self-consistent multimode lasing theory for complex or random lasing media, Phys. Rev. A **74**, 043822 (2006).

[47] I. Khanin, *Fundamentals of Laser Dynamics* (Cambridge University, Cambridge, England, 2006).

[48] G. Agrawal, Gain nonlinearities in semiconductor lasers: Theory and application to distributed feedback lasers, IEEE J. Quantum Electron. **23**, 860 (1987).

[49] S. E. Hodges, M. Munroe, J. Cooper, and M. G. Raymer, Multimode laser model with coupled cavities and quantum noise, J. Opt. Soc. Am. B **14**, 191 (1997).

[50] J. Martin-Regalado, F. Prati, M. San Miguel, and N. B. Abraham, Polarization properties of vertical-cavity surface-emitting lasers, IEEE J. Quantum Electron. **33**, 765 (1997).

[51] L. Lugiato, F. Prati, and M. Brambilla, *Nonlinear Optical Systems* (Cambridge University, Cambridge, England, 2015).

[52] A. Fiore and A. Markus, Differential gain and gain compression in quantum-dot lasers, IEEE J. Quantum Electron. **43**, 287 (2007).

[53] T. Fördös, K. Postava, H. Jaffrès, and J. Pištora, Matrix approach for modeling of emission from multilayer spin-polarized light-emitting diodes and lasers, J. Opt. **16**, 065008 (2014).

[54] K. Postava, T. Fördös, H. Jaffrès, L. Halagačka, H. J. Drouhin, and J. Pištora, Modeling of anisotropic grating structures with active dipole layers, Proc. SPIE **9516**, 95160O (2015).

[55] A. E. Siegman, *Lasers* (University Science Books, Mill Valley, CA, 1986).

[56] J. Frougier, G. Baili, M. Alouini, I. Sagnes, H. Jaffrès, A. Garnache, C. Deranlot, D. Dolfi, and J.-M. George, Control of light polarization using optically spin-injected vertical external cavity surface emitting lasers, Appl. Phys. Lett. **103**, 252402 (2013).

[57] L. Coldren, S. Corzine, and M. Mashanovitch, *Diode Lasers and Photonic Integrated Circuits*, Wiley Series in Microwave and Optical Engineering (Wiley, New York, 2012).

[58] P. E. Faria, Jr., G. Xu, J. Lee, N. C. Gerhardt, G. M. Sipahi, and I. Žutić, Toward high-frequency operation of spin lasers, Phys. Rev. B **92**, 075311 (2015).

[59] C. Henry, Theory of the linewidth of semiconductor lasers, IEEE J. Quantum Electron. **18**, 259 (1982).

[60] S. Balle, Simple analytical approximations for the gain and refractive index spectra in quantum-well lasers, Phys. Rev. A **57**, 1304 (1998).

[61] M. Sargent, M. Scully, and W. Lamb, *Laser Physics*, Advanced Book Program (Westview Press, Boulder, CO, 1978).

[62] A. Garnache, B. Sermage, R. Teissier, G. Saint-Giro, and I. Sagnes, A new kind of fast quantum-well semiconductor saturable-absorber mirror with low losses for ps pulse generation, in *Proceedings of the International Conference on Indium Phosphide and Related Materials, 2003* (IEEE, Piscataway, NJ, 2003), pp. 247–250.

[63] M. S. Park, B. T. Ahn, B.-S. Yoo, H. Y. Chu, H.-H. Park, and C. J. Chang-Hasnain, Polarization control of vertical-cavity surface-emitting lasers by electro-optic birefringence, Appl. Phys. Lett. **76**, 813 (2000).

[64] M. Herms, M. Fukuzawa, V. Melov, J. Schreiber, P. Möck, and M. Yamada, Residual strain in annealed GaAs single-crystal wafers as determined by scanning infrared polariscopy, X-ray diffraction and topography, J. Cryst. Growth **210**, 172 (2000).

[65] O. Krebs and P. Voisin, Giant Optical Anisotropy of Semiconductor Heterostructures with No Common Atom and The Quantum-Confined Pockels Effect, Phys. Rev. Lett. **77**, 1829 (1996).

[66] L. F. Lastras-Martínez, R. E. Balderas-Navarro, A. Lastras-Martínez, and K. Hingerl, Stress-induced optical anisotropies measured by modulated reflectance, Semicond. Sci. Technol. **19**, R35 (2004).

[67] O. Krebs, W. Seidel, J. P. André, D. Bertho, C. Jouanin, and P. Voisin, Investigations of giant "forbidden" optical anisotropy in GaInAs—InP quantum well structures, Semicond. Sci. Technol. **12**, 938 (1997).

[68] S. Cortez, O. Krebs, and P. Voisin, In-plane optical anisotropy of quantum well structures: From fundamental considerations to interface characterization and optoelectronic engineering, J. Vac. Sci. Technol. B **18**, 2232 (2000).

[69] S. Cortez, O. Krebs, and P. Voisin, Breakdown of rotational symmetry at semiconductor interfaces: A microscopic description of valence subband mixing, Eur. Phys. J. B **21**, 241 (2001).

[70] L. F. Lastras-Martínez, D. Rönnow, P. V. Santos, M. Cardona, and K. Eberl, Optical anisotropy of (001)-GaAs surface quantum wells, Phys. Rev. B **64**, 245303 (2001).

[71] E. A. Cerda-Méndez, R. E. Balderas-Navarro, A. Lastras-Martínez, L. F. Lastras-Martínez, A. Garnache, L. Cerutti, and A. Jouill, Interfaces in $Ga_x In_{1-x}As_y Sb_{1-y}/Al_x Ga_{1-x}As_y Sb_{1-y}$ multi-quantum-well heterostructures probed by transmittance anisotropy spectroscopy, J. Appl. Phys. **98**, 066107 (2005).

[72] H. Shen, M. Wraback, J. Pamulapati, P. G. Newman, M. Dutta, Y. Lu, and H. C. Kuo, Optical anisotropy in $GaAs/Al_x Ga_{1-x}As$ multiple quantum wells under thermally induced uniaxial strain, Phys. Rev. B **47**, 13933 (1993).

[73] *Handbook of Optical Constants of Solids I, II, III*, edited by E. D. Palik (Academic, New York, 1991).

[74] M. Bass, C. DeCusatis, J. Enoch, V. Lakshminarayanan, G. Li, C. MacDonald, V. Mahajan, and E. Van Stryland, *Handbook of Optics: Optical Properties of Materials, Nonlinear Optics, Quantum Optics (set)*, Handbook of Optics, 3rd ed. (McGraw-Hill, New York, 2009), Vol. 4.

[75] M. Schubert, V. Gottschalch, C. M. Herzinger, H. Yao, P. G. Snyder, and J. A. Woollam, Optical constants of Ga(x)In(1-x)P lattice matched to GaAs, J. Appl. Phys. **77**, 3416 (1995).

[76] T. Fördös, K. Postava, H. Jaffrès, J. Pištora, and H.-J. Drouhin, Mueller matrix ellipsometric study of multilayer spin-VECSEL structures with local optical anisotropy (unpublished) (2017).